

# A biophysical model of apple (Malus domestica Borkh.) and pear (Pyrus communis L.) fruit growth

**Biosystems Engineering** 

Dequeker, Bart; Šalagovič, Jakub; Retta, Moges; Verboven, Pieter; Nicolaï, Bart M. https://doi.org/10.1016/j.biosystemseng.2024.02.003

This publication is made publicly available in the institutional repository of Wageningen University and Research, under the terms of article 25fa of the Dutch Copyright Act, also known as the Amendment Tayerne.

Article 25fa states that the author of a short scientific work funded either wholly or partially by Dutch public funds is entitled to make that work publicly available for no consideration following a reasonable period of time after the work was first published, provided that clear reference is made to the source of the first publication of the work.

This publication is distributed using the principles as determined in the Association of Universities in the Netherlands (VSNU) 'Article 25fa implementation' project. According to these principles research outputs of researchers employed by Dutch Universities that comply with the legal requirements of Article 25fa of the Dutch Copyright Act are distributed online and free of cost or other barriers in institutional repositories. Research outputs are distributed six months after their first online publication in the original published version and with proper attribution to the source of the original publication.

You are permitted to download and use the publication for personal purposes. All rights remain with the author(s) and / or copyright owner(s) of this work. Any use of the publication or parts of it other than authorised under article 25fa of the Dutch Copyright act is prohibited. Wageningen University & Research and the author(s) of this publication shall not be held responsible or liable for any damages resulting from your (re)use of this publication.

For questions regarding the public availability of this publication please contact  $\frac{openaccess.library@wur.nl}{openaccess.library@wur.nl}$ 

ELSEVIER

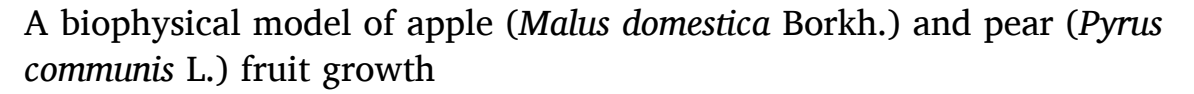
Contents lists available at ScienceDirect

# **Biosystems Engineering**

journal homepage: www.elsevier.com/locate/issn/15375110



# Research Paper



Bart Dequeker <sup>a</sup>, Jakub Šalagovič <sup>a</sup>, Moges Retta <sup>b</sup>, Pieter Verboven <sup>a,\*</sup>, Bart M. Nicolaï <sup>a,c</sup>

- <sup>a</sup> BIOSYST-MeBioS, KU Leuven, Willem de Croylaan 42, 3001, Leuven, Belgium
- b Department of Plant Sciences, Wageningen University and Research, Bornsesteeg 48, 6708PE, Wageningen, the Netherlands
- <sup>c</sup> Flanders Centre of Postharvest Technology, Willem de Croylaan 42, 3001 Leuven, Belgium

# ARTICLE INFO

# Keywords: Fruit growth model Water relations Xylem water potential Transport Carbohydrate uptake Malus domestica Pyrus communis Simulation

# ABSTRACT

Fruit mass and sugar content are important quality attributes of apple and pear fruit. During fruit growth, water and sugars accumulate as a result of the coordination of water and solid fluxes. This causes expansive growth driven by turgor pressure and controlled by cell mechanical properties. To analyse the effect of environmental conditions on fruit growth dynamics, a biophysical model of apple (Malus domestica Borkh.) and pear (Pyrus communis L.) fruit growth was developed and adapted from the Fishman-Génard model. Dynamically changing patterns of average fruit fresh mass, dry mass and soluble solid mass in response to the environmental conditions during multiple seasons of varying environmental conditions were well captured by a parameterised model for apple and pear fruit growth. Sensitivity analyses showed that the model was most sensitive to variations in parameters related to active transport, cell wall extensibility and plant water status. The model enabled the analysis of how fruit growth dynamics were affected by stress conditions. This model, which integrates biophysical laws and parameters governing fruit water and solute dynamics, may serve as a basis to investigate the role of the processes involved in the complex growing behavior of pome fruit, and to optimise and predict fruit growth and quality.

## 1. Introduction

The growth of pome fruit such as apple (Malus domestica Borkh.) and pear (Pyrus communis L.) is the consequence of two separate processes: cell division and cell expansion (Janssen et al., 2008; Rodríguez, Sánchez, & De La Casa, 2011; Tijero, Girardi, & Botton, 2021). Most of the post-anthesis cell divisions occur during the early stages of growth. Cell expansion, in contrast, continues through the cell division period until harvest and is driven by active transport of carbohydrates to fruit cells from photosynthesis, with sorbitol as the predominant transport carbohydrate. These photosynthates are used in the synthesis of structural carbohydrates for growth, respiration, energy storage and metabolism into other sugars (most notably sucrose and fructose), starch and organic acids, such as malic acid (Berüter, 1990; Berüter et al., 1997). Along with the accumulation of sugars, the osmotic potential drops and growing cell walls are loosened, causing transitorily reduced cell wall stresses and turgor pressure. In response, water flows into the cell and restores turgor pressure and wall stresses, resulting in enlarged cells (Cosgrove, 2016).

During these growth stages, accumulation of matter and increase of fruit tissue volume are determined by the balance of incoming and outgoing flows of water and carbohydrates (Lang, 1990). These fluxes are the result of tightly coordinated and regulated processes such as vascular (xylem and phloem) transport, sugar unloading and metabolism, deposition of new cell wall material and cell wall expansion driven by turgor pressure (Lockhart, 1965). The processes governing these flows depend on the developmental stage, the degree of between-fruit competition, genotypic and hormonal effects, and external conditions, such as light intensity, temperature and water availability. More specifically, the water status of fruit and tree driving these transport processes have been reported to determine fruit yield, composition and sugar concentration (Morandi et al., 2012, 2014; Naor, Klein, & Doron, 1995; Nemeskéri, 2007; Shackel, 2007; Wada et al., 2021).

Understanding and modeling fruit growth patterns can aid in providing predictions for fruit quality and timing of orchard management. Multiple authors have presented models of pome fruit growth for prediction of fruit quality and harvest date by fitting mathematical functions to experimental measurements (Lakso et al., 1995; Martins

E-mail address: pieter.verboven@kuleuven.be (P. Verboven).

 $<sup>^{\</sup>ast}$  Corresponding author.

#### $P_{v,sat}$ , $P_{v,act}$ Water vapour pressure of saturated air, ambient air Nomenclature Variable Definition $P_{x,min}$ , $P_{x,max}$ Minimum and maximum daily xylem water potential Ratio of xylem and phloem area to fruit area (-) (MPa) $A_x$ , $A_p$ , $A_f$ Surface area of xylem, phloem, fruit (cm<sup>2</sup>) $\Pi_x$ , $\Pi_p$ , $\Pi_f$ , $\Pi_{o,p}$ , $\Pi_{o,f}$ Osmotic pressure in xylem, phloem, fruit; $C_{\rm p},\,C_{\rm f},\,C_{\rm mb}$ Concentration of sugar in the phloem, fruit, over the osmotic pressure of other solutes in phloem, fruit (MPa) membrane (g $g^{-1}$ ) $\Delta P$ Vapour pressure deficit (VPD) (MPa) $C_{\mathrm{p,min}},\,C_{\mathrm{p,max}}$ Minimum, maximum phloem sugar concentrations (g Growth respiration coefficient (-) $q_{ m gr}$ $g^{-1}$ ) Maintenance respiration coefficient (h<sup>-1</sup>) $q_{\rm ma, 293}$ $Q_{10}$ , $Q_{10,a}$ Temperature ratio of maintenance respiration, active Parameter of surface area to fruit mass function (cm<sup>2</sup> g<sup> $-\eta$ </sup>) γ $d_{\mathrm{f}}$ Fruit diameter (cm) transport (-) Ε Cell wall elastic modulus (MPa) Gas constant (cm<sup>3</sup>MPa K<sup>-1</sup>mol<sup>-1</sup>) R Parameter of surface area to fruit mass function (-) $R_{\rm f}$ Fruit respiration (g h<sup>-1</sup>) GDDGrowing degree days (°d) Mass density of water, dry mass (g cm<sup>-3</sup>) $\rho_{\rm w}$ , $\rho_{\rm s}$ Surface permeability to water vapour (cm h<sup>-1</sup>) h $S_{p}$ Sensitivity coefficient (-) $H_{\rm f},\,H_{\rm act}$ Relative humidity of fruit, ambient air (-) Reflection coefficient of the composite membrane for sugar $\sigma_{\rm x}$ , $\sigma_{\rm p}$ Rate constant of xylem functionality, cell wall extensibility $k_{\rm x}, k_{\varphi}$ uptake of xylem, phloem (-) $(h^{-1})$ Time (h) Maximum rate of active transport per unit of dry mass $k_{s,\text{max}}$ T Temperature (°C) $(g g^{-1}h^{-1})$ Reference temperature for GDD calculation (°C) $T_{\rm base}$ Michaelis-Menten constant for active uptake (-) $K_{\mathrm{M}}$ $T_{\rm min,day}$ , $T_{\rm max,day}$ Lowest, highest temperature during the day (°C) Fruit length (cm) l<sub>f</sub> $T_{\rm f}$ Fruit transpiration (g $h^{-1}$ ) $L_{x,\text{max}}$ Maximum conductivity ratio of xylem vs. phloem (−) Kinetic parameter of active transport (h) Hydraulic conductivity of xylem, phloem Mass flow of water in the xylem, phloem (g $h^{-1}$ ) $L_{\rm x}$ , $L_{\rm p}$ $U_{\rm x}$ , $U_{\rm p}$ (g cm<sup>-2</sup> MPa<sup>-1</sup> h<sup>-1</sup>) $U_{\rm s}$ , $U_{\rm a}$ , $U_{\rm m}$ , $U_{\rm d}$ Mass flow of solids; active transport, mass flow, $m_{\rm w}$ , $m_{\rm s}$ , $m_{\rm ss}$ Mass of water, solid, soluble solids (g) passive diffusion (g h<sup>-1</sup>) $m_{\rm w,0}, m_{\rm s,0}$ Initial water mass (g), initial solid mass (g) VFruit volume (cm<sup>3</sup>) $M_{\rm s}$ Molecular mass of sugar (g mol<sup>-1</sup>) Y Threshold pressure for growth (MPa) Permeability of composite membrane for sugar transport Cell wall extensibility (MPa<sup>-1</sup>h<sup>-1</sup>) $p_{\rm s}$ $\varphi$ $(g cm^{-2}h^{-1})$ Maximum cell wall extensibility (MPa-1h-1) $\varphi_{\rm max}$ $P^*$ Saturation pressure (MPa) Ratio of soluble solids to solids (-) $P_x$ , $P_p$ , $P_f$ Hydrostatic pressure in the xylem, phloem, fruit (MPa) $P_{\rm f,0}$ Initial fruit turgor pressure (MPa)

et al., 2008; Ribeiro et al., 2017; Zadravec et al., 2014). However, these models are algebraic descriptions, which do not provide further insight into the processes involved and do not take into account environmental effects. Because water and dry mass accumulation during expansive growth are governed by multiple connected mechanisms and depend on environmental factors, process-based fruit growth models have been proposed as useful frameworks to advance the understanding of the development of fruit quality in response to environment and orchard management (Génard et al., 2007).

To investigate this complexity, biophysical models of fruit growth (Bussières, 1994; Génard et al., 2003, 2007; Lescourret, Ben Mimoun, & Génard, 1998; Marcelis et al., 2009) have been developed to describe the main processes involved in the development of fruit quality during growth. The model proposed by (Fishman & Génard, 1998) was further modified and used to analyse the effect of climate fluctuations and horticultural management on fruit quality of several species, including peach (Léchaudel et al., 2005; Lechaudel et al., 2007), tomato (Constantinescu, 2020; Liu et al., 2007; Van de Wal, 2017), kiwifruit (Hall et al., 2013), grape (Van de Wal, 2017; Zhu et al., 2019) and blueberry (Jorquera-Fontena, Génard, & Franck, 2017). Cakpo et al. (2020) modeled sugar and starch dynamics during growth for several fruit species. To our knowledge, biophysical fruit growth models of fresh mass, dry mass, and sugars in response to varying environmental conditions have not been developed for apple and pear fruit.

The goal of this study was to develop a biophysical fruit growth model of apple and pear fruit based on the model of Fishman and Génard (1998) to analyse and simulate seasonal variations in fruit quality, namely fresh mass, dry mass, and soluble solids, in response to the

differences in environmental conditions for four different growing seasons. The model was modified, adapted and parametrised to account for the growth physiology of apple and pear fruit. These adaptations include developmental age-dependent changes in sugar accumulation, fruit transpiration, and cell extensibility, as well as plant water status as a function of environmental conditions. The model was used to analyse the dominant fluxes and water status of fruit and tree, allowing the study of diurnal and whole-season fruit growth dynamics. This model enabled the investigation of fruit growth dynamics and fruit water status in response to simulated water and phloem sugar stresses, exploring the impact of management practices and stresses during apple and pear fruit growth.

# 2. Materials and methods

# 2.1. Plant material

Experimental data were collected from Jonagold apple trees (*Malus domestica* Borkh. 'Jonagold') planted in 2014 and Conference pear trees (*Pyrus communis* L. 'Conference') planted in 1963, growing in the orchards of Proefcentrum Fruitteelt vzw (pcfruit) in Sint-Truiden, Belgium (lat. 50° 46′ 21.9" N, long. 5° 9′ 36.4" E) on loamy soil. Regular horticultural care was applied, including thinning, pruning and control of pests and diseases according to recommended practices for each fruit variety. Local weather data, including relative humidity, temperature and vapour pressure deficit (*VPD*) were measured hourly during each season by a meteorological station close to the orchards at pcfruit. Fig. 1 and Table 1 compare the environmental conditions during the growing

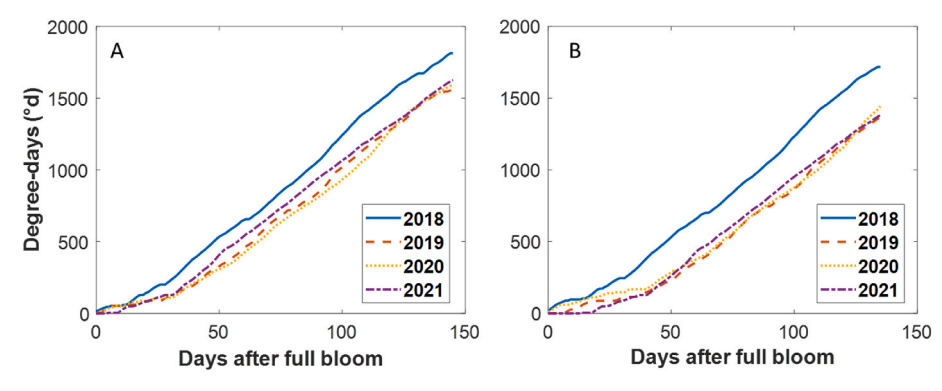


Fig. 1. Cumulative growing degree days for apple (A) and pear (B) during the seasons of 2018–2021. Growing degree days (GDD, in °d) were calculated using equation (1).

Table 1 Environmental conditions during the growing seasons (from the day of full bloom to the end of the season) for apple and pear of 2018–2021. For each season, the following weather parameters are given: the day of full bloom (DOFB), average temperature ( $T_{avg}$ ), maximum temperature ( $T_{max}$ ), minimum temperature ( $T_{min}$ ), average relative humidity ( $RH_{avg}$ ), total rainfall (in mm), average daily rainfall (mm), total irradiation (W h m<sup>-2</sup>) and average daily irradiation (W h m<sup>-2</sup>).

Apple									
Year	DOFB	T <sub>avg</sub> (°C)	T <sub>max</sub> (°C)	T <sub>min</sub> (°C)	RH <sub>avg</sub> (%)	Total rainfall (mm)	Rainfall (daily average) (mm)	Total irradiation (W h $\mathrm{m}^{-2}$ )	Irradiation (daily average) (W h $\mathrm{m}^{-2}$ )
2018	22/ 04	18.0	36.9	1.4	69.5	212.6	1.42	7.2 10 <sup>5</sup>	4783.3
2019	20/ 04	16.3	41.6	-1.4	69.7	255.4	1.70	7.6 10 <sup>5</sup>	5089.0
2020	16/ 04	16.7	38.3	-2.9	66.1	185.8	1.24	7.8 10 <sup>5</sup>	5209.1
2021	28/ 04	15.8	33.6	-2.1	79.2	515.7	3.03	7.1 10 <sup>5</sup>	4191.5
Pear									
Year	DOFB	T <sub>avg</sub> (°C)	T <sub>max</sub> (°C)	T <sub>min</sub> (°C)	RH <sub>avg</sub> (%)	Total rainfall (mm)	Rainfall (daily average) (mm)	Total irradiation (W h $m^{-2}$ )	Irradiation (daily average) (W h $\mathrm{m}^{-2}$ )
2018	19/ 04	18.3	36.9	1.4	68.4	207.4	1.60	6.5 10 <sup>5</sup>	4985.0
2019	10/ 04	15.6	41.6	-2.5	68.0	211.6	1.63	6.7 10 <sup>5</sup>	5167.4
2020	07/ 04	16.4	38.3	-2.9	62.7	148.2	1.14	7.2 10 <sup>5</sup>	5524.6
2021	19/ 04	15.7	33.6	-2.5	76.4	448.9	3.20	6.6 10 <sup>5</sup>	4746.8

seasons of apple and pear. Growing degree days (GDD, in °d) were calculated for each day as in equation (1):

$$GDD = \begin{cases} \frac{T_{\text{max,day}} + T_{\text{min,day}}}{2} - T_{\text{base}} & T_{\text{min,day}} > T_{\text{base}} \\ 0 & T_{\text{min,day}} \le T_{\text{base}} \end{cases}$$

$$(1)$$

in which  $T_{\rm min,day}$  and  $T_{\rm max,day}$  (°C) are the lowest and highest temperature during that day respectively, and  $T_{\rm base}$  is the reference temperature and was set to 5 °C (Christodoulou & Culham, 2021; Łysiak, 2022).

# 2.2. Fruit quality measurements

During four growing seasons from 2018 to 2021, 10 fruit per variety were harvested at weekly intervals during the cell expansion phase up to fruit maturation. Apples and pears were picked at eye level using random selection, while omitting underdeveloped and damaged fruit. Fresh mass of harvested fruit was determined with a digital scale. The fruit maximum equatorial diameter and length were measured using a digital caliper and were used to estimate fruit surface area with equations (2) and (3). Fruit dry mass was measured by drying a small cortex tissue sample in an oven at 70 °C until its mass reached equilibrium. Fruit water mass was calculated as the difference between fresh and dry

mass. The total soluble solid content was determined with a handheld refractometer (PR-101  $\alpha$ , ATAGO CO. LTD, Tokyo, Japan; Quick-Brix 60, Mettler Toledo International Inc., Columbus, USA) and was converted to soluble solid mass following the method proposed by Hall et al. (2006). Fruit osmotic potential was determined from freezing point osmometry for the 2021 season. A subsample from the fruit was frozen with liquid nitrogen, crushed with mortar and pestle, and was subsequently ground into a fine powder with a grinding mixer (Mixer mill 200 MM, Retsch GmbH, Haan, Germany). The obtained powder was centrifuged at 24 000 g for 15 min, after which the liquid fraction was collected. Next, the osmolarity of the liquid fraction was measured with a freezing point osmometer (Osmomat 3000, Gonotec GmbH, Berlin, Germany) and converted to osmotic potential with the van 't Hoff equation (Nobel, 1974). Before measuring, the device was calibrated with distilled water (zero osmolarity), and two solutions of known osmolarity.

# 2.3. Fruit skin water permeability

The fruit skin permeability was determined by measuring fruit transpiration rate on harvested fruit as described by Fishman and Génard (1998). The fruit pedicel was removed and the wound was sealed with grease (Van de Wal, 2017). At the start of the experiment,

the surface area of each fruit was estimated based on formulas (2) and (3), with  $A_{\rm f}$  (cm<sup>2</sup>) the fruit surface area,  $d_{\rm f}d_{\rm f}$  (cm) the fruit diameter and  $l_{\rm f}$  (cm) the pear fruit length.

$$A_{\rm f,apple} = 4\pi \left(\frac{d_{\rm f}}{2}\right)^2 \tag{2}$$

$$A_{\rm f,pear} = 2\pi \left(\frac{d_{\rm f}}{2}\right)^2 + \pi \left(\frac{d_{\rm f}}{2}\right) \sqrt{\left(\frac{d_{\rm f}}{2}\right)^2 + \left(l_{\rm f} - \left(\frac{d_{\rm f}}{2}\right)\right)^2} \tag{3}$$

The maximum equatorial diameter and length of the fruit were measured using a digital caliper. Next, fruit were placed in an incubator (Termaks KBP 6087, LED Techno nv, Heusden-Zolder, Belgium) with controlled temperature and humidity (20  $^{\circ}$ C, 52% RH). The mass of each fruit was measured for 6 h at intervals of 45 min. The mass loss observations, the fruit surface area and ambient air temperature and humidity were used to estimate the fruit skin permeability for five replicates at weekly intervals during the season of 2021 with equation (18).

# 2.4. Xylem midday water potential

The midday branch water potential of the tree branch was measured during the season of 2021 using a pressure chamber (Model 670, PMS Instrument Company, Albany, USA) following the method in (Levin, 2019). The chosen leaves were mature, fully expanded and all measurements were made between 12:00 and 13:00 Central European Time (CET). Leaf samples (n = 6-10) were selected randomly from a set of 10 trees for each variety and were covered with reflective foil-laminate plastic bags for 45 min to allow equilibration before excision. After this period, each leaf was cut from the branch with a sharp blade, placed in the pressure chamber through a seal and subjected to a constant pressure increase below 0.5 bar s<sup>-1</sup>. The pressure value at the first appearance of water from the cut during pressurisation was taken as the midday xylem water pressure. The obtained xylem water pressure values were related to the vapour pressure deficit, calculated from the measurements of air temperature and relative humidity from a weather station of the research station. The vapour pressure deficit  $\Delta P$  (MPa) was calculated as the difference between the water vapour pressure of saturated air  $P_{v,sat}$  (MPa) and the actual vapour pressure  $P_{v,act}$  (MPa).

$$\Delta P = P_{v,sat} - P_{v,act} \tag{4}$$

The partial water vapour pressure was expressed as a function of relative humidity  $H_{\rm act}$  (between 0 and 1) and  $P_{\rm v,sat}$ :

$$P_{v,act} = P_{v,sat} H_{act} \tag{5}$$

The Buck equation (Buck, 1981) was used to calculate the saturation vapour pressure as a function of temperature T (K), assuming the fruit and air share the same temperature:

$$P_{v,\text{sat}} = 0.61121 \exp\left[\left(18.678 - \frac{T - 273.15}{234.5}\right) \left(\frac{T - 273.15}{257.14 + (T - 273.15)}\right)\right]$$
(6)

# 2.5. Model description

The fruit growth model was an adaptation of a biophysical representation of fruit growth originally developed for peach (Fishman & Génard, 1998). The model simulates the growth after cell division has ceased. The growth model assumes that the fruit can be considered as one compartment (a cell community with a constant number of growing cells) separated by a composite membrane from the environment and branch. The main variables of the system are the water mass  $m_{\rm w}$  (g) and the dry mass  $m_{\rm s}$  (g) in the fruit flesh, and fruit turgor pressure  $P_{\rm f}$  (MPa). Water and dry matter dynamics during fruit growth are described by balance equations governed by biophysical transport processes and irreversible cell expansion as a consequence of turgor pressure

(Lockhart, 1965; Ortega, 1985, 1990). The model with the main fluxes and variables is illustrated in Fig. 2.

#### 2.5.1. Water balance and fluxes

The rate of change of water in the fruit over time is the sum of the water influx from the xylem  $U_x$  (g h<sup>-1</sup>) and phloem  $U_p$  (g h<sup>-1</sup>) minus the water loss through transpiration  $T_f$  (g h<sup>-1</sup>).

$$\frac{dm_{\rm w}}{dt} = U_{\rm x} + U_{\rm p} - T_{\rm f} \tag{7}$$

The indices x, p and f refer to xylem, phloem and fruit, respectively. The water flow from the vasculature into the fruit is driven by the differences in hydrostatic pressure P (MPa) and osmotic pressures  $\Pi$  (MPa) between phloem or xylem and the fruit.

$$U_{x} = A_{x}L_{x}(P_{x} - P_{f} - \sigma_{x}(\Pi_{x} - \Pi_{f}))$$

$$\tag{8}$$

$$U_{\rm p} = A_{\rm p} L_{\rm p} (P_{\rm p} - P_{\rm f} - \sigma_{\rm p} (\Pi_{\rm p} - \Pi_{\rm f})) \tag{9}$$

where  $A_x$  and  $A_p$  are the xylem and phloem membrane area (cm²), and with  $L_x$  and  $L_p$  (g cm⁻² MPa⁻¹ h⁻¹) the hydraulic conductivity of xylem and phloem membrane respectively. The effective reflection coefficient of the phloem and xylem, denoted  $\sigma_p$  and  $\sigma_x$ , are dimensionless measures of the impermeability of each membrane to solutes. The concentration of solutes in the xylem, and, hence,  $\Pi_x$ , was considered negligible compared to inside the fruit.  $\sigma_x$  was set to 1, since the plasma membrane is considered impermeable to sugars (Knipfer & Fricke, 2010). The membrane areas of xylem and phloem were assumed to increase proportionally to the fruit area  $A_f$  (cm²) through a proportionality constant a (dimensionless).

$$A_{\rm x} = a A_{\rm f} \tag{10}$$

$$A_{\rm p} = a A_{\rm f} \tag{11}$$

An empirical equation was used to relate fruit surface area  $A_f$  to fresh mass, with coefficients  $\gamma$  (cm<sup>2</sup> g<sup>- $\eta$ </sup>) and  $\eta$  (-) as fitting parameters:

$$A_{\rm f} = \gamma (m_{\rm w} + m_{\rm s})^{\eta} \tag{12}$$

The osmotic pressures were calculated from the concentrations of

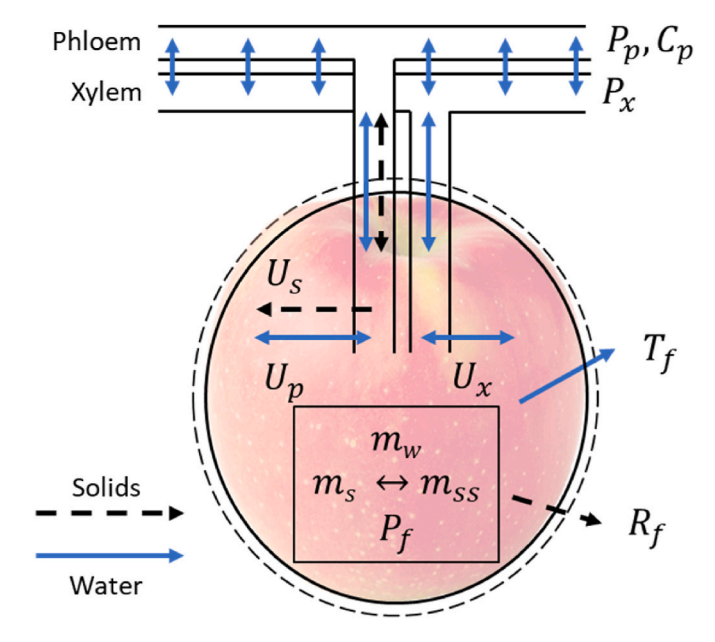


Fig. 2. Schematic representation of the fruit growth model (adapted from Hall et al. (2013). The different fluxes of solids (dashed arrows) and water (solids arrows) are shown.

sugars C (g g<sup>-1</sup>) based on the van 't Hoff equation (Nobel, 1974) with equation (13), with gas constant R (83.14 cm<sup>3</sup> MPa K<sup>-1</sup> mol<sup>-1</sup>) and temperature T (K). The contribution to osmotic pressure of solutes other than carbohydrates (such as amino acids and minerals) was accounted for with a term  $\Pi_o$  (MPa).

$$\Pi = \Pi_{\rm o} + R \ T \frac{C}{(1 - C)M_{\rm s}} \tag{13}$$

where  $M_{\rm s}$  (g mol<sup>-1</sup>) is the molecular mass of the most abundant sugar which was assumed to be sorbitol in the phloem, and hexoses in the fruit (Berüter et al., 1997). As a first approximation,  $\Pi_{\rm o}$  was chosen constant during fruit development. The sugar concentration  $C_{\rm f}$  (g g<sup>-1</sup>) was calculated based on the soluble solutes. It was assumed that a proportion Z (dimensionless) of the total content of accumulated carbohydrates remains as soluble sugars whereas the rest is converted to structural material (14). The soluble solids content  $m_{\rm ss}$  (g) was, hence, derived in a simplified approach to represent soluble solids dynamics.

$$m_{\rm ss} = Zm_{\rm s} \tag{14}$$

$$C_{\rm f} = \frac{m_{\rm ss}}{m_{\rm o} + m_{\rm o}} \tag{15}$$

The proportion Z was modeled as an empirical function of fruit mass, derived from measurements, with  $Z_1$  and  $Z_2$  dimensionless fitting parameters:

$$Z = Z_1(m_w + m_s) + Z_2 (16)$$

For pear, the hydraulic conductivity of xylem was assumed constant. For apple, however, it was assumed to decrease with time based on the observation that the pedicel hydraulic conductivity declined during ripening as a consequence of physical disruption of the xylem vessels (Dražeta et al., 2004; Morandi et al., 2011, 2012). As there is no evidence for breakdown in phloem functionality during fruit development, phloem conductivity was considered constant. These assumptions then yield equation (17) for  $L_x$ :

$$L_{\mathbf{x}} = \frac{2L_{\mathbf{x},\max}}{1 + e^{k_{\mathbf{x}}t}} L_{\mathbf{p}} \tag{17}$$

where  $L_{x,\max}$  (dimensionless) is the maximum conductivity ratio between xylem and phloem and  $k_x$  (h<sup>-1</sup>) a parameter describing the changes in xylem functionality over time t (h). The value of  $L_{x,\max}$  was based on the ratio of xylem and phloem flows.

Transpiration water loss is driven by the difference in relative humidity between the air filled space in the fruit  $H_{\rm f}$  (dimensionless) and the ambient atmosphere  $H_{\rm act}$  (dimensionless). Additionally, transpiration is considered proportional to the fruit surface area  $A_{\rm f}$  and the permeability of its surface to water vapour h (cm  $h^{-1}$ ), as shown in (18).

$$T_f = A_f \alpha h \left( H_f - H_{\text{act}} \right) \tag{18}$$

where  $\alpha = \frac{M_w P^*}{RT}$ , with  $M_w$  the molecular mass of water (g mol<sup>-1</sup>),  $P^*$  the saturation pressure (MPa), R the gas constant (cm<sup>3</sup> MPa K<sup>-1</sup>mol<sup>-1</sup>) and T temperature in K. The temperature dependence of saturation vapour pressure was implemented as in Fishman and Génard (1998), with dimensionless constants  $P_1^*$  equal to 8.048  $\times$  10<sup>-3</sup> and  $P_2^*$  equal to 0.0547 (equation (19)).

$$P^* = P_1^* e^{P_2^* (T - 273.15)} ag{19}$$

Fruit surface water vapour permeability decreases with increasing fruit mass, which is in agreement with measurements presented in this work and as reported by (Lang, 1990; Maguire et al., 2000). This trend was implemented with empirical equations: based on our experiments, a power function (20) was used for apple, and a rational function (21) was used for pear.

$$h = h_1 (m_{\rm w} + m_{\rm s})^{h_2} \tag{20}$$

$$h = \frac{h_1}{(m_{\rm w} + m_{\rm s}) + h_2} \tag{21}$$

where  $h_1$  and  $h_2$  are fitted parameters. For apple, the units of  $h_1$  and  $h_2$  are cm  $h^{-1}g^{-h_2}$  and (–) respectively. For pear, the units of  $h_1$  and  $h_2$  are cm  $h^{-1}g$  and g respectively.

# 2.5.2. Carbohydrate balance and fluxes

The accumulation of dry matter with time is the uptake from the phloem  $U_s$  (g h<sup>-1</sup>) minus respiration  $R_f$  (g h<sup>-1</sup>).

$$\frac{dm_{\rm s}}{dt} = U_{\rm s} - R_{\rm f} \tag{22}$$

The transport of dry matter from the phloem to the fruit  $U_s$  was calculated with equation (23) as the sum of active transport  $U_a$  (g h<sup>-1</sup>), mass flow  $U_m$  (g h<sup>-1</sup>) and passive diffusion  $U_d$  (g h<sup>-1</sup>).

$$U_{\rm s} = U_{\rm a} + U_{\rm m} + U_{\rm d} \tag{23}$$

Dry matter transport from phloem to fruit by mass flow was calculated from equation (24). Passive diffusion due to the gradient of sugar concentrations between phloem and fruit was calculated with equation (25):

$$U_{\rm m} = (1 - \sigma_{\rm p}) C_{\rm mb} U_{\rm p} \tag{24}$$

$$U_{\rm d} = A_{\rm p} p_{\rm s} (C_{\rm p} - C_{\rm f}) \tag{25}$$

with  $p_s$  (g cm<sup>-2</sup> h<sup>-1</sup>) the permeability of the composite membrane to sugar transport and  $C_{\rm mb}$  (g g<sup>-1</sup>) the mean concentration of the solutes in the membrane contributing to mass flow (equation (26)):

$$C_{\rm mb} = \frac{C_{\rm p} + C_{\rm f}}{2} \tag{26}$$

The rate of active carbohydrate uptake  $U_a$  was described with a modified Michaelis-Menten equation, with  $K_M$  the Michaelis constant (dimensionless). The maximum uptake rate was made proportional to dry mass  $m_s$ , maximum uptake rate  $k_{s,max}$  (g g<sup>-1</sup>h<sup>-1</sup>) and temperature T through the  $Q_{10}$  concept with  $Q_{10,a}$  (dimensionless) (Fishman and Génard, 1998; Hall et al., 2013).

$$U_{\rm a} = \frac{m_{\rm s} \ Q_{10,\rm a}^{\frac{7-293}{10}}}{\left(1 + e^{\frac{t-7}{12}}\right)} \frac{k_{\rm s,max} \ C_{\rm p}}{K_{\rm M} + C_{\rm p}}$$
(27)

In (27),  $\tau_1$  (h) and  $\tau_2$  (h) are kinetic parameters accounting for an "inhibitory" effect which increases with fruit age, and hence time t (h). This assumption was based on the decreasing accumulation of sugars in later stages of growth per gram of apple fruit (Li et al., 2018) and pear fruit (Oikawa et al., 2015). Sugar signals have been shown to mediate plant sugar regulation, the effects of which depend on developmental stage and environmental conditions (Matsoukas, Massiah, & Thomas, B., 2013; Rolland, Baena-gonzalez, & Sheen, 2006).

Dry mass loss is driven by fruit respiration, and consists of growth respiration and maintenance respiration (equation (28)). Growth respiration  $R_f$  is proportional to dry mass uptake rate via growth coefficient  $q_{\rm gr}$  (dimensionless), while maintenance respiration depends on dry mass and the maintenance respiration coefficient  $q_{\rm ma}$  (h<sup>-1</sup>). This coefficient was made dependent on temperature through  $Q_{10}$ , relative to  $q_{\rm ma,293}$  (h<sup>-1</sup>), the maintenance coefficient at reference temperature 20 °C or 293 K, as shown in equation (29).

$$R_{\rm f} = q_{\rm gr} \frac{dm_{\rm s}}{dt} + q_{\rm ma} m_{\rm s} \tag{28}$$

$$q_{\rm ma} = q_{\rm ma,293} Q_{10}^{\frac{7-293}{10}} \tag{29}$$

#### 2.5.3. Volume growth

The balance equations were connected to the rate of change of fruit volume  $V(\mathrm{cm}^3)$  to solve for the fruit turgor pressure. The fruit volume change can be written as the sum of the rates of change of water and dry mass:

$$\frac{dV}{dt} = \frac{1}{\rho_{\rm w}} \frac{dm_{\rm w}}{dt} + \frac{1}{\rho_{\rm s}} \frac{dm_{\rm s}}{dt} \tag{30}$$

where  $\rho_{\rm w}$  (g cm  $^{\!-3}$  ) and  $\rho_{\rm s}$  (g cm  $^{\!-3}$  ) are the density of water and carbohydrates, respectively.

Two different approaches were used to obtain an expression for turgor pressure: (I) by only taking into account plastic deformations, and (II) by including elastic and plastic changes to volume. Both calculation methods were used to assess the impact of elasticity on the transport processes determining fruit growth.

Fruit volume change can be calculated from the Lockhart equation (Lockhart, 1965) for irreversible plant growth, when the elastic deformations and the contribution of dry mass to volume changes are neglected (Fishman & Génard, 1998):

$$\frac{dV}{dt} = \begin{cases} V\varphi(P_f - Y) & P_f > Y \\ 0 & 0 < P_f < Y \end{cases}$$
 (31)

with  $\varphi$  the cell wall extensibility (MPa<sup>-1</sup>h<sup>-1</sup>) and Y the threshold pressure of fruit turgor (MPa) above which irreversible expansion occurs. Under the aforementioned assumptions, and by setting (30) and (31) as equal, the turgor pressure  $P_f$  can then be obtained from the resulting analytical equation, as shown in eq. (32):

$$P_{\rm f} = \frac{A_{\rm x}L_{\rm x}\left(P_{\rm x} + \Pi_{\rm f}\right) + A_{\rm p}L_{\rm p}\left(P_{\rm p} - \sigma_{\rm p}\left(\Pi_{\rm p} - \Pi_{\rm f}\right)\right) - T_{\rm f} + \rho_{\rm w}V\varphi Y}{A_{\rm x}L_{\rm x} + A_{\rm p}L_{\rm p} + \rho_{\rm w}V\varphi} \tag{32}$$

Alternatively, the change of volume can also be expressed as the result of volume variations due to plastic and elastic deformations (Ortega, 1985), with *E* the elastic modulus (MPa).

$$\frac{dV}{dt} = \frac{1}{E} V \frac{dP_{\rm f}}{dt} + \begin{cases} V \varphi (P_{\rm f} - Y) & P_{\rm f} > Y \\ 0 & 0 < P_{\rm f} < Y \end{cases}$$
 (33)

In this case, fruit turgor pressure is expressed by combining eq. (30) and eq. (33) as a differential equation, as proposed in (Lechaudel et al., 2007), that can be solved numerically.

$$\frac{dP_{\rm f}}{dt} = \frac{E}{V} \left( \frac{1}{\rho_{\rm w}} \frac{dm_{\rm w}}{dt} + \frac{1}{\rho_{\rm s}} \frac{dm_{\rm s}}{dt} - V\varphi(P_{\rm f} - Y) \right) \qquad if \quad P_{\rm f} > Y 
\frac{dP_{\rm f}}{dt} = \frac{E}{V} \left( \frac{1}{\rho_{\rm w}} \frac{dm_{\rm w}}{dt} + \frac{1}{\rho_{\rm s}} \frac{dm_{\rm s}}{dt} \right) \qquad if \quad 0 < P_{\rm f} < Y$$
(34)

Cell wall extensibility  $\varphi$  was assumed to follow an exponential decrease in time, determined by the parameters  $\varphi_{\rm max}$  (MPa<sup>-1</sup>h<sup>-1</sup>) and  $k_{\varphi}$  (h<sup>-1</sup>), as  $\varphi$  tends to become zero for mature cells (Proseus, Ortega, & Boyer, 1999). The declining extensibility is consistent with the decreasing activity of cell wall polysaccharide modifying enzymes (Dheilly et al., 2016), involved in the regulation of the cell wall mechanical properties and growth processes (Cosgrove, 1993, 2016).

$$\varphi = \frac{2\varphi_{\text{max}}}{1 + e^{k_{\varphi^I}}} \tag{35}$$

# 2.5.4. Model inputs and initial conditions

The model requires inputs of two environmental variables (temperature and relative humidity of the ambient air) and two variables related to the stem vasculature (the xylem water potential and phloem sugar concentration).

Xylem water potential and phloem sugar concentration were modeled to reflect the influence of time of day and environmental conditions by letting the daily pattern vary between set daily minimum and maximum values with the model of (Parton & Logan, 1981). The daily patterns follow a sinusoidal function with the highest phloem sugar concentration  $C_{\rm p,max}$  (g g<sup>-1</sup>) and lowest xylem water potential  $P_{\rm x,min}$  (MPa) at solar noon, and lowest phloem sugar concentration  $C_{\rm p,min}$  (g g<sup>-1</sup>) and highest xylem water potential  $P_{\rm x,max}$  (MPa) between sunset and sunrise for that day (Fig. 1). For xylem water potential,  $P_{\rm x,min}$  was related to environmental conditions based on an experimental regression between vapour pressure deficit  $\Delta P$  and midday stem water potential  $P_{\rm x,min}$ , measured from the pressure bomb experiments, with  $P_1$  and  $P_2$  (MPa) fitting parameters.

$$P_{\text{x,min}} = P_1 \ln(\Delta P) + P_2 \tag{36}$$

To initialise the growth model, the model requires fruit water mass, dry mass and turgor pressure at the beginning of the simulation at a specific time point. The average water mass  $m_{\rm w,0}$  (g) and dry mass  $m_{\rm s,0}$  (g) were input as the initial values of simulation for each growing season, knowing also initial time since the specific day after full bloom. The initial turgor pressure  $P_{\rm f,0}$  (MPa) was set based on observed values at fruit set, and was calculated as the difference of the water potential measured with the method from 2.4 and the osmotic potential of the fruit.

#### 2.5.5. Model solution, parameterisation and calibration

The system of ordinary differential equations (ODEs) was solved numerically in MATLAB R2020a (The Mathworks Inc., Natick, USA), using the ode45 solver with adaptive time steps. Relative error tolerance was set to  $10^{-3}$  and absolute error tolerance was set to  $10^{-6}$ . Simulations were run for the same time period as the time of experimental data collection. Fig. S1 gives the simulation period for each season, together with their initial conditions. For apple, this time period corresponds to the time from about 40 to 60 DAFB, until about 150–170 DAFB. For pear, simulations were run from between about 50 and 70 DAFB, until about 130–140 DAFB. The weather data needed to calculate the environmental conditions as described in 2.5.4, and the initial values of the state variables were entered as inputs for simulation.

Model parameters were estimated from experimental data as described above or taken from the literature. Parameter values are given in Table S1, with the source of the values. The parameters that were not determined in independent experiments, were estimated with model calibration by fitting simulated curves to experimental values of dry and fresh mass data. Model implementation and parameter estimations were done in OptiPa, a modeling tool for calibrating models based on ordinary differential equations (Hertog et al., 2007). For parameter estimations, non-linear least squares optimisation Levenberg-Marquardt method was performed for both fresh and dry mass simultaneously. For both apple and pear simulations, seasons 2018 to 2020 were included in the calibration dataset, while data from the 2021 season was used for validation. Four parameters were obtained through model calibration:  $L_p$ ,  $\tau_1$ ,  $\tau_2$  and  $k_{\varphi}$ . The goodness of fit of the model was evaluated through the root mean square error (RMSE) and relative root mean squared error (RRMSE), which was formulated as:

$$RRMSE = \frac{1}{\bar{y}} \sqrt{\frac{\sum_{i=1}^{N} n_i (y_{i,\text{sim}} - \bar{y}_{i,\text{data}})^2}{\sum_{i=1}^{N} n_i}}$$
(37)

with N the number of dates on which fruit were sampled,  $n_i$  the number of repetitions at instance i,  $y_{i,\text{sim}}$  the simulated fruit fresh or dry mass at instance i,  $\overline{y}_{i,\text{data}}$  the mean value of measured data at instance i, and  $\overline{y}$  the mean of all measured values.

# 2.5.6. Sensitivity analysis

A sensitivity analysis was performed to assess the sensitivity of the model to parameter variations. For each parameter during the sensitivity

analysis, the default value as presented in Table S1 was changed between -50 % and +50 %, while all other parameter values were kept unchanged. The sensitivity of the model to a parameter was quantified by the normalised sensitivity coefficient  $S_P$ , defined as the ratio between the variation of fruit dry or fresh mass  $(\Delta y)$  relative to its average value  $(\bar{y})$  and the variation of the parameter values  $(\Delta p)$  relative to its average value  $(\bar{p})$  (equation (38)).

$$S_P = \frac{\Delta y/\overline{y}}{\Delta p/\overline{p}} \tag{38}$$

Mean normalised sensitivity coefficients were calculated over the whole range of percentage changes for each parameter. The fresh mass or dry mass at the end of a simulated growth season was used as the test variable, applying conditions from 2018.

#### 2.5.7. Fruit growth dynamics simulated under stress conditions

The model was applied to analyse the effect of virtual phloem sugar and xylem water potential stresses on fruit growth dynamics. Model sensitivity to input variations was calculated as described in 2.5.6. In addition, the responses to phloem sugar stress and to xylem water potential stresses were analysed, as these stress conditions may reflect horticultural interventions in the production of photosynthates (for instance with shading nets) and in the water status of the tree (for example drought periods or withholding of irrigation). Phloem sugar stress was simulated by decreasing the phloem sugar concentration lower and upper limits by 0.05 g g $^{-1}$  based in first approximation on the ranges used in (Fishman & Génard, 1998). Water stress was simulated by reducing the xylem water potential by 0.25 MPa - chosen based on observations between 0.1 and 0.5 MPa during prolonged drought stress by Bhusal, Han, and Yoon (2019) – while relative air humidity was kept unchanged. These simulated stresses were applied for 3 weeks early in the season (60 DAFB) and late in the season (110 DAFB).

# 3. Results

# 3.1. Environmental conditions during growing seasons

Considerable differences were observed between the environmental conditions during multiple growing seasons from 2018 to 2021. Fig. 1 shows that the 2018 season had higher cumulative growing degree-days compared to the other seasons. Furthermore, Table 1 highlights the differences in temperature, humidity, rainfall and radiation between the seasons. The 2018 season had the highest average temperature (18  $^{\circ}\text{C})$  of seasons 2018 to 2021, while the 2021 season was on average the coldest (15.8  $^{\circ}\text{C})$ . During the 2021 season, the highest relative humidity and rainfall were observed. Solar irradation was the lowest during the 2021 season and the highest during the 2020 season.

# 3.2. Model parameters

Estimated values for the fruit surface water vapour permeability were found to decrease with increasing fruit mass and, hence, fruit age, for both apple and pear ( $R^2 = 0.91$  and  $R^2 = 0.87$ , respectively), as can be seen in Fig. 3. Similar observations have been made by (Jones & Higgs, 1982) for other apple cultivars. The decrease in h occurred more rapidly during development for apple than for pear. The values at the end of development for apple and pear were within the range of values for apple fruit (0.876-127 cm  $h^{-1}$ ) reported by Maguire et al. (2000).

The estimated values of the hydraulic conductivity  $L_p$  of the phloem surface area were 0.080 g cm<sup>-2</sup> MPa<sup>-1</sup> h<sup>-1</sup> for apple and 0.206 g cm<sup>-2</sup> MPa<sup>-1</sup> h<sup>-1</sup> for pear, assuming for both a constant ratio of composite membrane area to fruit area (a) of 0.0273 as in Fishman and Génard (1998). They were comparable to the value used by Fishman and Génard (1998) for maize roots (0.0972 g cm<sup>-2</sup>MPa<sup>-1</sup>h<sup>-1</sup>), blueberries (0.04583 g cm<sup>-2</sup>MPa<sup>-1</sup>h<sup>-1</sup>; Jorquera-Fontena et al., 2017), tomatoes (0.15 g cm<sup>-2</sup>MPa<sup>-1</sup>h<sup>-1</sup>; Liu et al., 2007) and mentioned by Nobel (1974) for plant membranes (0.2664 g cm<sup>-2</sup> MPa<sup>-1</sup> h<sup>-1</sup>).

Values for midday xylem water potential  $P_{x,min}$  in apple and pear tree branches were found to decrease with increasing  $\Delta P$  and to plateau for high  $\Delta P$  (Fig. 4). These observations were modeled as a logarithmic function of  $\Delta P$  (equation (36)). Similar relationships were reported for young apple trees (De Swaef, Steppe, & Lemeur, 2009). The midday stem water potential values reported here were consistent with values between -1 MPa and -2 MPa) for apple (Naor et al., 1995; Šircelj et al., 2005) and between -0.4 and -1.5 MPa for pear (Vélez-Sánchez, Balaguera-López, & Rodríguez Hernández, 2022).

The value for the time constant of the exponential decrease in cell wall extensibility  $k_{\varphi}$  was estimated as 0.0029 h<sup>-1</sup> for apple and 0.0027 h<sup>-1</sup> for pear, for both varieties assuming a maximum extensibility  $\varphi_{\text{max}}$  of 0.1 MPa<sup>-1</sup>h<sup>-1</sup>. With these calibrated values for  $k_{\varphi}$ ,  $\varphi$  showed a consistent decline to zero towards maturity at the end of the season (Fig. S2), reflecting the biological and physical changes in cell walls of mature cells (Proseus et al., 1999).

From Fig. 5A it appears that the proportion of soluble solids to total solids Z was not strongly influenced by increasing fruit fresh mass for apple. While the linear regression fit yielded a slope with a value of 6.25  $\times$   $10^{-4}$  which differed significantly from zero (p < 0.05),  $R^2$  was in that case equal to 0.238. Therefore, the ratio Z was considered constant in the model ( $Z_1=0,Z_2=0.49$ ). For pear, in contrast, a moderate linear trend ( $R^2=0.63$ ) was observed (Fig. 5B). This was implemented as a linear function, with estimated values of 0.0020 and 0.24 for  $Z_1$  and  $Z_2$ , respectively. The obtained values for Z were similar in magnitude to the value of 0.61 for peach (Fishman and Génard, 1998) and 0.52 for tomato by (Liu et al., 2007), assuming Z constant during fruit growth.

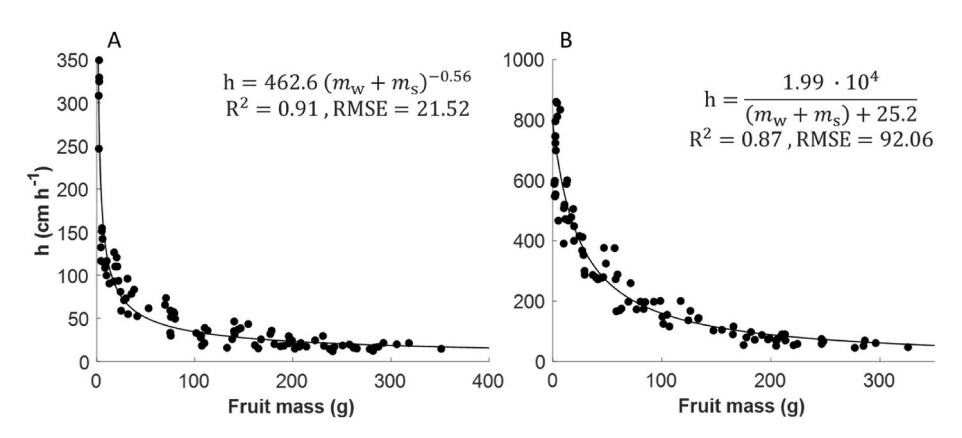


**Fig. 3.** Fruit surface water vapour permeability as a function of fruit mass, for apple (A) and pear (B). Fitted functions versus fruit fresh mass ( $m_w + m_s$ ) (line) to the measurements (symbols) are shown. In addition, the  $R^2$  and RMSE of the fitted functions are given.

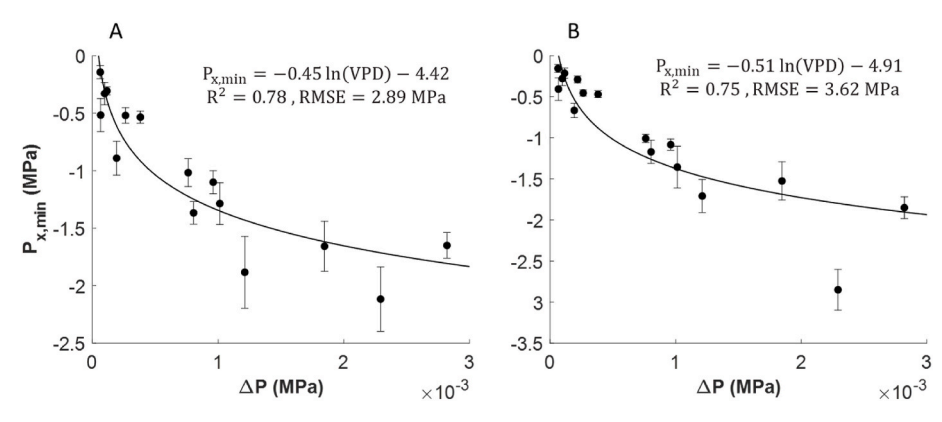


**Fig. 4.** Midday xylem water potential as a function of vapour pressure deficit (VPD) for apple (A) and pear (B), with logarithmic functions (line) fitted to the measurements (symbols). Standard deviations for measurements (n = 6-10) are shown as vertical bars. In addition, the  $R^2$  and RMSE of the fitted functions are given.

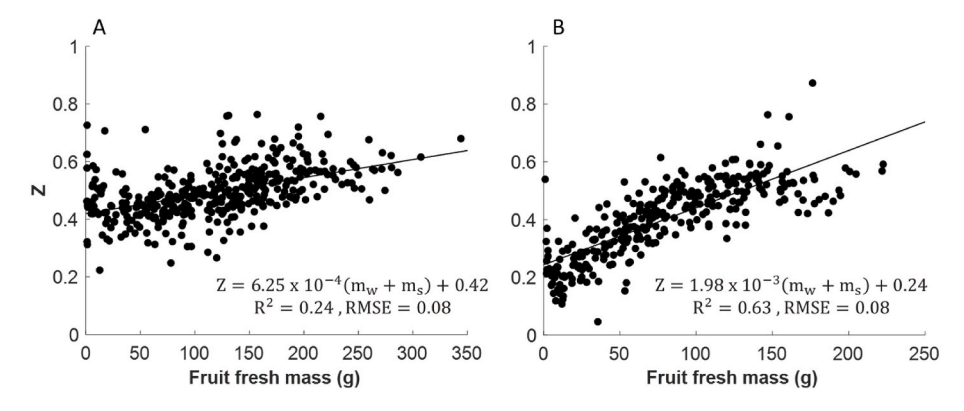
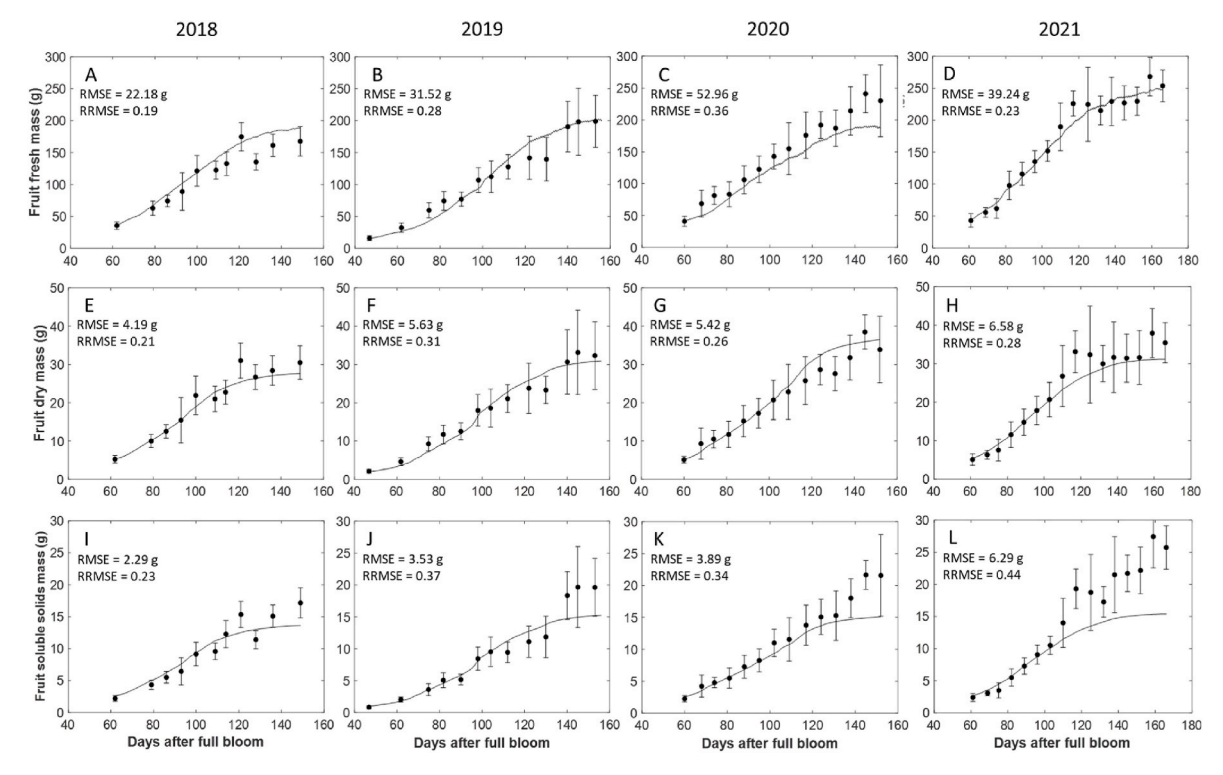


Fig. 5. The ratio of soluble solids to solids for apple (A) and pear (B). Linear fits versus fruit fresh mass  $(m_w + m_s)$  (line) to the data (symbols) for which fitting parameters  $R^2$  and RMSE values are shown, are displayed.



**Fig. 6.** Simulation results of the fruit growth model for apple. Seasons 2018 to 2020 were used in model calibration, season 2021 was used for model validation. Measured (symbols) and simulated (lines) dynamics of apple fruit fresh mass (A, B, C, D), fruit dry mass (E, F, G, H) and soluble solids mass (I, J, K, L) for each season are shown. Standard deviations for measurements (n = 10) are shown as vertical bars. For each curve, *RMSE* and *RRMSE* are indicated.

The values for  $\tau_1$  and  $\tau_2$  for the active transport equation (27) were estimated as 1502.6 h and 468.3 h for apple, respectively, and 1914.9 h and 797.0 h for pear, respectively.

# 3.3. Simulations of fruit fresh mass, dry mass and soluble solid mass

Measurements and simulations of fresh mass, dry mass and soluble sugars for seasons 2018 to 2021 are shown in Fig. 6 for apple and in Fig. 7 for pear. Seasons 2018, 2019; 2020 were used as calibration set and season 2021 as validation set. For apple (Fig. 6), in general, the sigmoidal shape of the growth curve was reproduced by the model. RMSE and RRMSE values were between 22.2 and 53.0 g and 0.19-0.36 for fruit fresh mass, respectively (Fig. 6A-C), and between 4.2 and 5.6 g and 0.21-0.31 for fruit dry mass, respectively (Fig. 6E-G). For soluble solid mass (Fig. 6I-K), RMSE and RRMSE were between 2.3 and 3.9 g and 0.23-0.37, respectively. Fresh mass was underestimated in year 2020 (Fig. 6C) and soluble solid mass was underestimated in 2019 and 2020 (Fig. 6J and K), notably at the end of the season. A good correspondence between measurements and simulations was found in 2021 for fruit fresh mass (Fig. 6D, RMSE of 39 g and RRMSE of 0.23) and fruit dry mass (Fig. 6H, RMSE of 6.6 g and RRMSE of 0.28). The soluble solids mass from the middle to the end of the season was underestimated (Fig. 6L), resulting in a high RMSE (6.3 g) and RRMSE (0.44).

For pear, the model was able to recreate the overall growth trends during each season (Fig. 7). The values of RMSE and RRMSE ranged between 22.8 and 35.7 g and 0.25–0.45, respectively, for fruit fresh mass (Fig. 7A–C), and between 3.9 and 4.8 g and 0.24–0.29, respectively, for fruit dry mass (Fig. 7E-G). A notable underestimation of fruit fresh mass was observed for the 2019 season (Fig. 7B). For fruit soluble solid mass (Fig. 7I–K) the RMSE and RRMSE were between 2.1 and 3.5 g and 0.27–0.43, respectively. The simulations of the validation dataset of the 2021 growing season showed a good match with the measurements, except for moderate underestimations at the end of the season (Fig. 7D–L). These simulations had RMSE and RRMSE values of 35.3 g

and 0.30 for fresh mass, 5.7 g and 0.34 for dry mass, and 3.5 g and 0.37 for soluble solid mass.

### 3.4. Parameter sensitivity analysis

The mean normalised sensitivity coefficients showed the different sensitivities of the simulated fruit water mass (Fig. 8A) and dry mass (Fig. 8B) of apple with respect to parameter fluctuations.

The model simulations for water mass were highly sensitive to variations in parameters related to active uptake of dry mass ( $\tau_2$ ;  $k_{\rm s,max}$ ,  $m_{\rm s,0}$ ), cell wall extensibility ( $k_{\varphi}$ ), phloem transport ( $\sigma_{\rm p}$  and Z) and xylem water potential ( $P_1$  and  $P_2$ ). Moreover, moderate sensitivity was observed for variations in the daily limiters of  $C_{\rm p}$  ( $C_{\rm p,min}$  and to a lesser extent  $C_{\rm p,max}$ ),  $\eta$  and  $K_{\rm m}$ . In contrast, small changes to the water mass simulations were induced by variations in transpiration function parameters ( $h_1$  and  $h_2$ ), xylem water potential upper limit  $P_{\rm x,max}$ , phloem conductivity  $L_{\rm p}$ , osmotic pressure parameters ( $\Pi_{\rm o,p}$  and  $\Pi_{\rm o,f}$ ), initial water mass  $m_{\rm w,0}$ , maximum extensibility  $\varphi_{\rm max}$ , yield pressure Y, initial turgor  $P_{\rm f,0}$  and elasticity E. For dry mass simulations, the model yielded particularly large changes in active transport parameters ( $\tau_2$ ,  $k_{\rm s,max}$ ,  $m_{\rm s,0}$ ,  $\sigma_{\rm p}$  and  $K_{\rm M}$ ). Moderate sensitivity was found for  $C_{\rm p,max}$ , while weak sensitivity was observed for the other model parameters.

# 3.5. Analysis of main processes of apple and pear fruit growth

To investigate the involvement of the different processes affecting fruit functioning during growth, the model simulations of the main fluxes and physiological parameters were analysed.

The relative contributions of the different fluxes to the water balance changed over the course of the season (Fig. 9A and E for apple, and Fig. 9B and F for pear), resulting in different growth rates at different times during the season. For the case of apple, xylem water transport was considered negligible (see equation (17)) and the main influx of

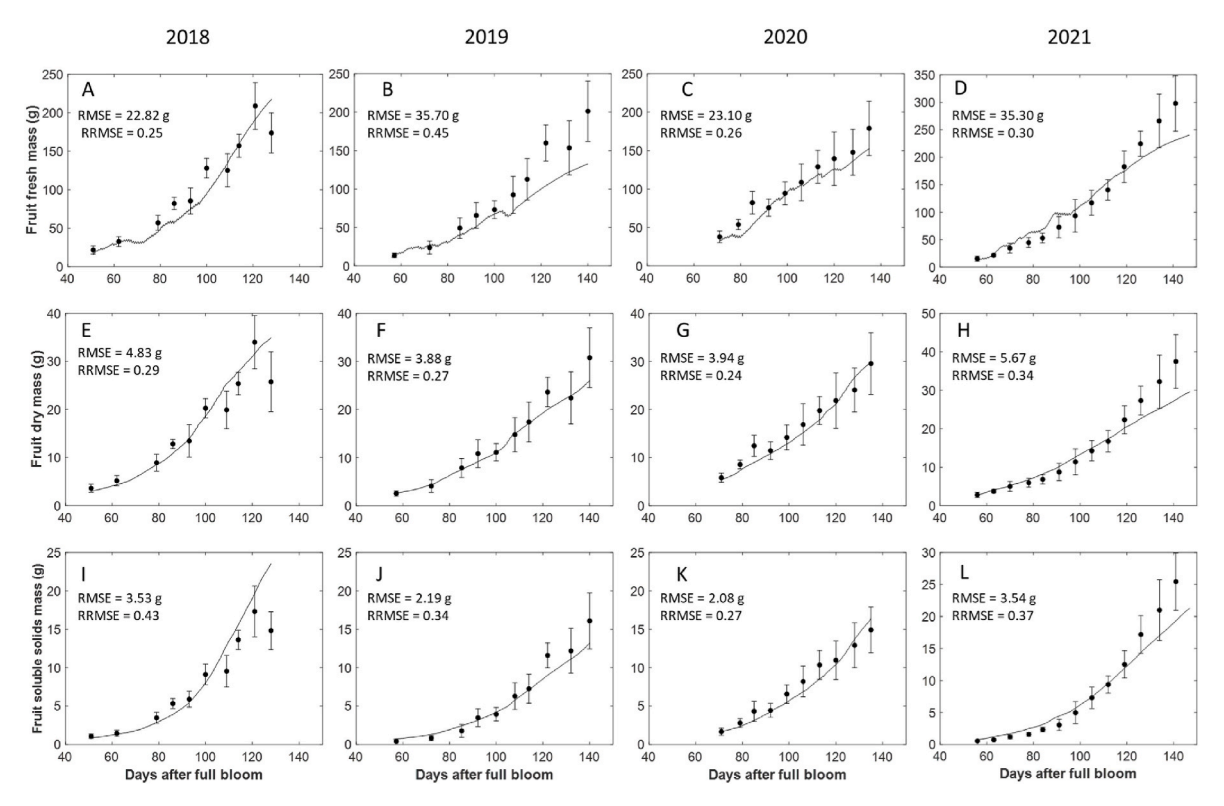


**Fig. 7.** Simulation results of the fruit growth model for pear. Seasons 2018 to 2020 were used in model calibration, season 2021 was used for model validation. Measured (symbols) and simulated (lines) dynamics of apple fruit fresh mass (A, B, C, D), fruit dry mass (E, F, G, H) and soluble solids mass (I, J, K, L) for each season are shown. Standard deviations for measurements (n = 10) are shown as vertical bars. For each curve, *RMSE* and *RRMSE* are indicated.

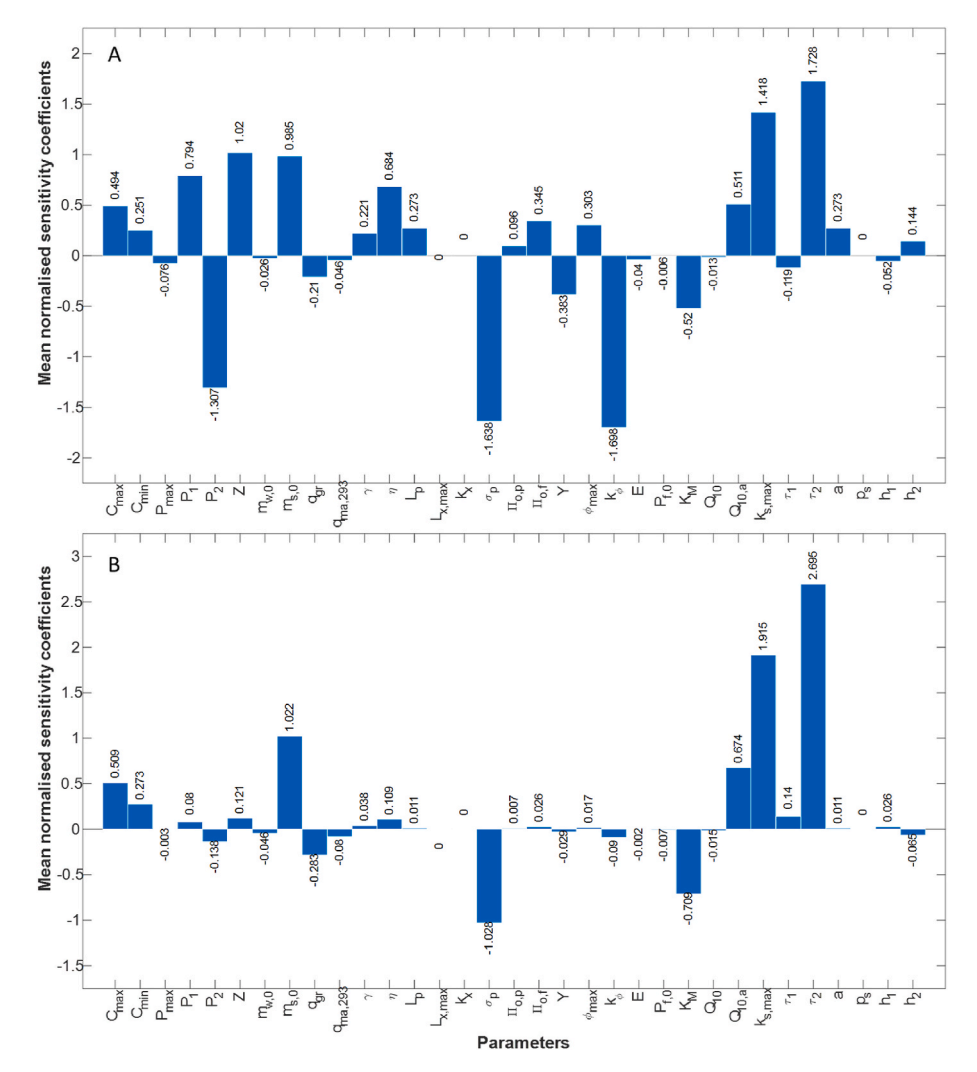


Fig. 8. Mean normalised sensitivity coefficients (bars) calculated for the final fruit fresh mass (A) and dry mass (B) at 120 DAFB to variations in parameters included in the apple fruit growth model. For each parameter, the default value as presented in Table S1 was changed with steps of 20% between -50% and +50%.

water was through the phloem. For pear fruit simulations, both xylem and phloem contributed to the water influx into the fruit.

The model reproduced the diurnal dynamics of fruit, showing the differences between night-time and midday periods (Fig. 9C and G for apple and Fig. 9D and H for pear). During the night, the water balance was positive, as the main water import from xylem and phloem exceeded the reduced transpiration water loss. During the midday period, the water balance decreased and sometimes became negative, resulting in a decrease in fruit mass. Overall the simulations showed that fruit mass growth would predominantly occur during the night.

The elastic deformation of fruit tissue was shown to have a large impact on the water fluxes to the fruit and the diurnal dynamics of growth. For apple (Fig. 9E and G), model simulations taking into account elasticity produced water influxes that would briefly become negative at noon, which resulted in a negative water balance around midday. In contrast, without elasticity, the water fluxes and consequently the water balance would generally not reach negative values. For pear on the other hand (Fig. 9D and H), negative water balances were predicted with and without consideration of elasticity, with stronger oscillations in the water balance when elasticity was included. Predominantly phloem flow became negative and shift the simulated water balance towards negative values at noon.

The simulated dry mass accumulation featured a maximum accumulation rate at around 110 DAFB for apple, after which dry mass accumulation would decline (Fig. 10A). For pear (Fig. 10B), the

accumulation of dry mass increased up to around 120 DAFB and would stay at a plateau for the remainder of the season. Fruit dry mass simulations (Fig. 10C and D) also showed circadian growth patterns, as dry mass accumulation would be the highest at around noon; the magnitudes of the dry mass accumulation fluxes were typically an order of magnitude smaller than those of the water fluxes.

Over the course of the season, fruit turgor pressure simulations showed a marked increase, with high values up to around 1.2 MPa for apple (Fig. 11A and B) and 1.5 MPa for pear (Fig. 11D and E). The turgor pressure at the end of the season was not influenced by changes in  $\Pi_{0.f}$ ,  $\Pi_{0,p}$  or  $P_{f,0}$  (data not shown). In contrast, turgor pressure in apple fruit has been reported to range between 0.2 and 0.8 MPa (Berüter, 1990; Iwanami et al., 2008; Wada et al., 2021). Model simulations predicted that the osmotic pressure of apple would not increase during growth, but decrease from about 1.8 MPa to about 1.6 MPa (Fig. 11A and B). This did not correspond to experimental observations reported in this work (Fig. 11C), where it would increase from 0.5 MPa for fruitlets to about 1.5 MPa at maturity, and to reports in literature (Berüter, 1990). The simulated osmotic pressure in pear increased over the course of the season, from around 1.2 MPa to about 2 MPa (Fig. 11D and E). This was consistent with fruit osmotic pressure measurements, which yielded osmotic pressure values early in the season of about 1 MPa, and values at the end of the season of 1.7 MPa (Fig. 11F).

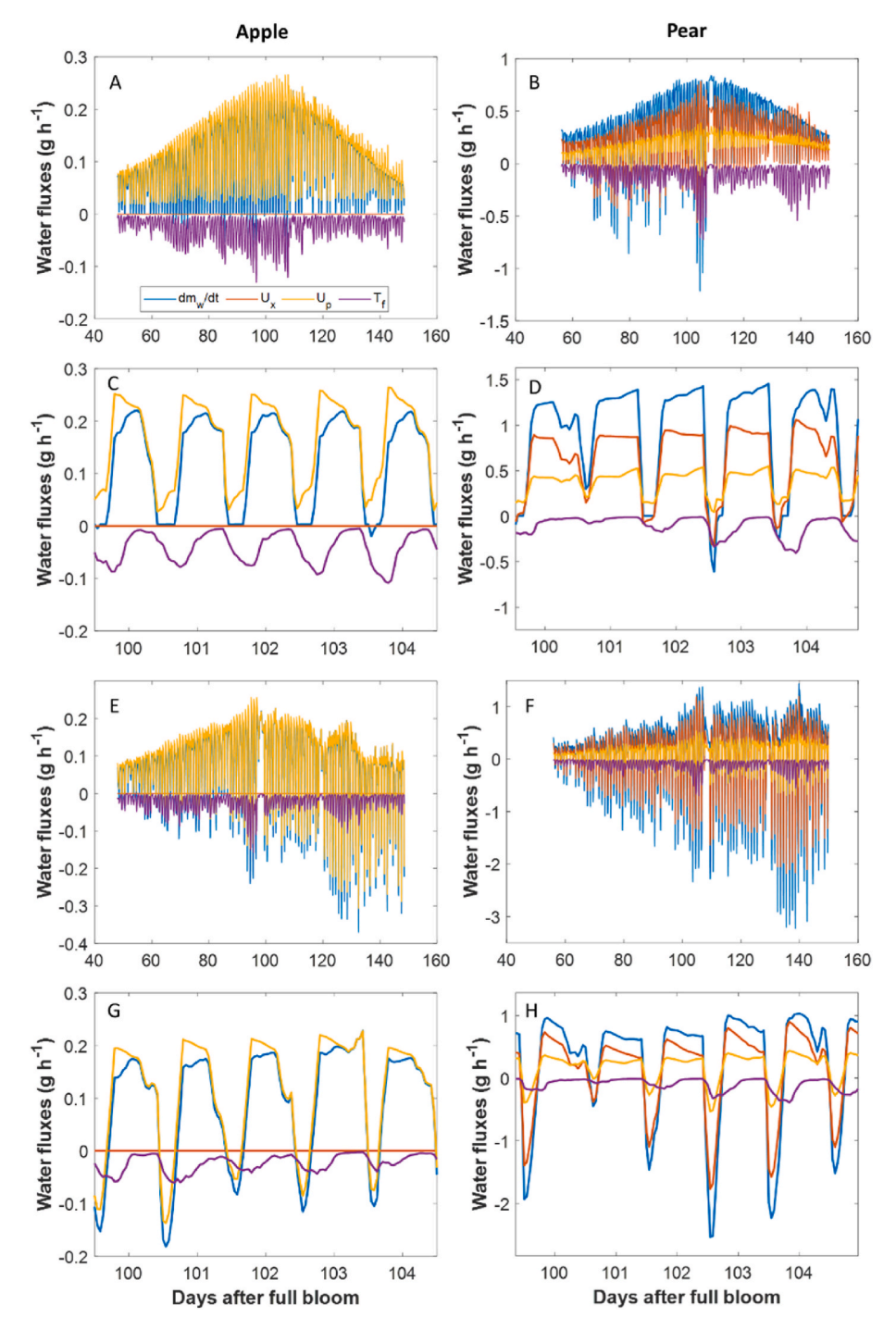


**Fig. 9.** Simulated profiles of the main water fluxes for the apple (A, C, E and G) and pear (B, D, F and H) fruit growth model. Water fluxes during the season, without elasticity in the model, are shown for apple (A) and pear (B), with a selected period from 100 to 104 DAFB shown for apple (C) and pear (D). Water fluxes during the season, with elasticity in the model, are shown for apple (E) and pear (F), with a selected period from 100 to 104 DAFB shown for apple (G) and pear (H). Blue:  $\frac{dm_v}{dt}$ ; orange:  $U_x$ ; Yellow:  $U_0$ ; purple:  $T_t$ . (For interpretation of the references to colour in this figure legend, the reader is referred to the Web version of this article.)

# 3.6. Fruit growth dynamics during simulated stresses

The effect of simulated stresses on the main factors driving fruit growth was studied with the model. The mean normalised sensitivity coefficients for fruit water and dry mass are presented in Fig. 12. The model showed limited sensitivity to temperature, and almost no sensitivity to relative air humidity. In contrast, high sensitivity coefficients were found for phloem sugar concentration and for xylem water potential with respect to fruit water mass.

The fruit growth dynamics in response to imposed water and phloem

sugar stresses were studied with the model, and are shown in Fig. 13. Lower phloem sugar concentrations directly resulted in lower active transport (equation (27)). As a consequence, the fruit osmotic pressure and in turn the xylem and phloem mass flows declined (equations (8) and (9)). The simulations gave a reduction in xylem mass flow (-16% during early stress and -2% during late stress), phloem mass flow (-31% during early stress and -24% during late stress), respiration (-29% during early stress and -24% during late stress), and a small difference in transpiration (-3% during early stress and -1% during late stress) and in osmotic pressure (-2% during early and -4% during

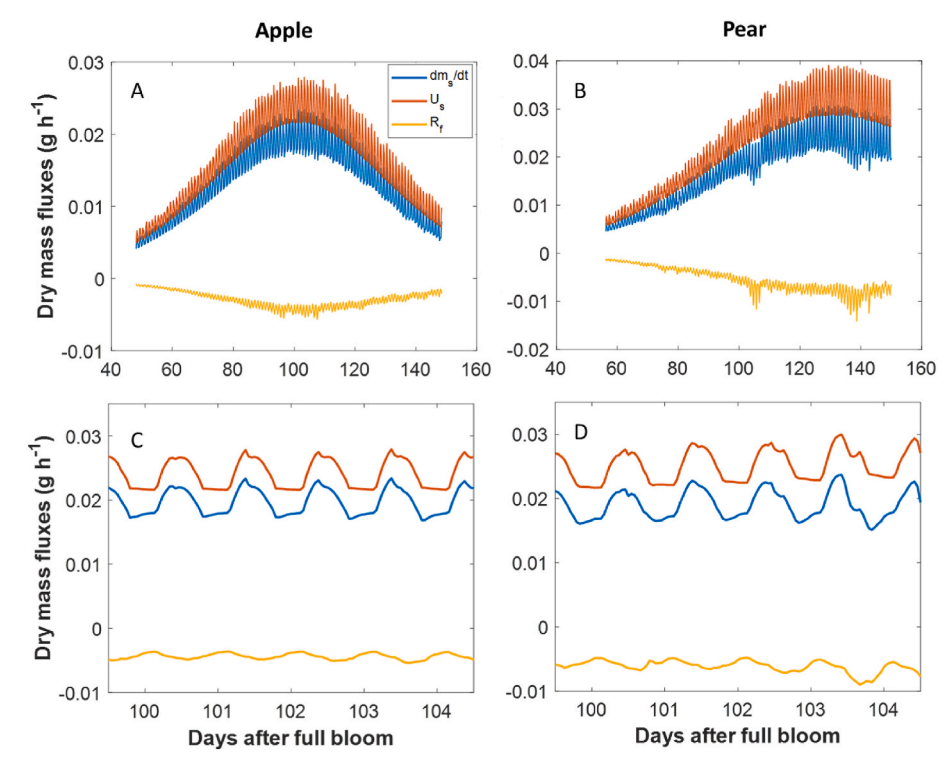


**Fig. 10.** Simulated profiles of the main dry mass fluxes for the apple (A and C) and pear (B and D) fruit growth model. Dry mass fluxes during the season are shown for apple (A) and pear (B), with a selected period from 100 to 104 DAFB shown for apple (C) and pear (D). Blue:  $\frac{dm_s}{dt}$ ; orange:  $U_s$ ; Yellow:  $R_f$ . (For interpretation of the references to colour in this figure legend, the reader is referred to the Web version of this article.)

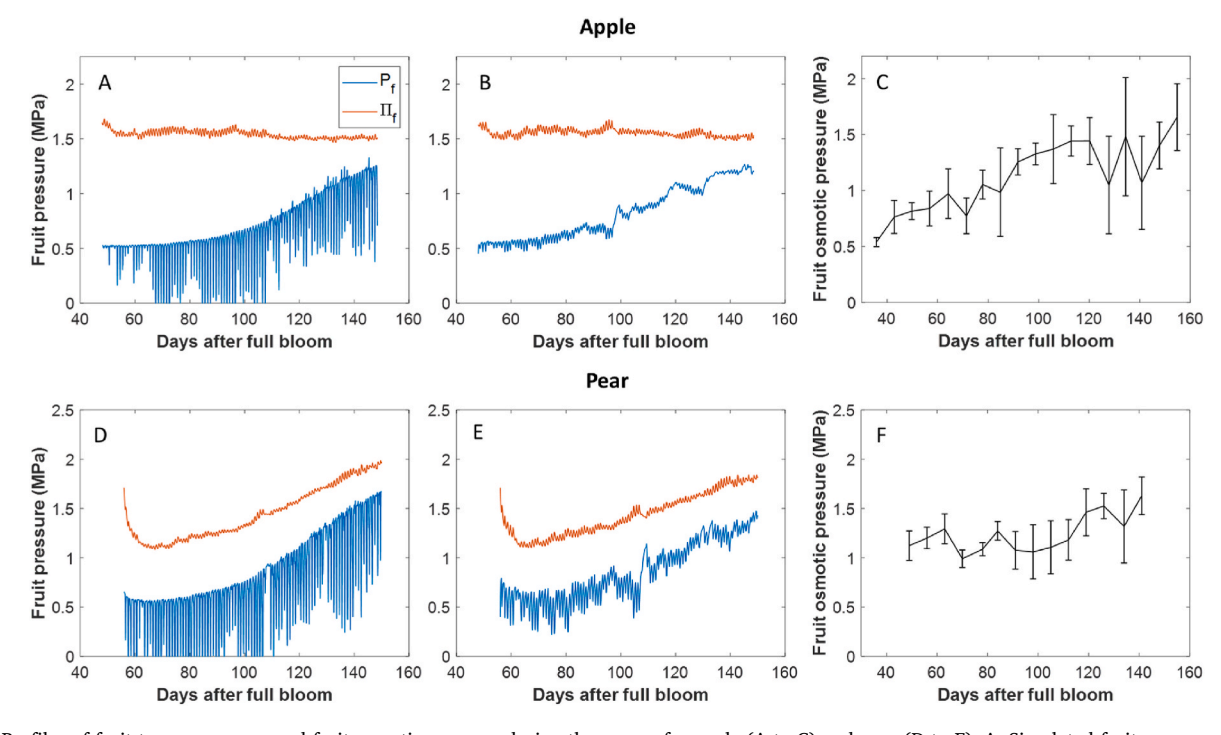


**Fig. 11.** Profiles of fruit turgor pressure and fruit osmotic pressure during the season for apple (A to C) and pear (D to F). A: Simulated fruit pressures for apple, without elasticity in the model. B: Simulated fruit pressures for apple, with elasticity included in the model. C: Measured fruit osmotic pressure of apple fruits during the season. D: Simulated fruit pressures for pear, without elasticity in the model. E: Simulated fruit pressures for pear, with elasticity included in the model. F: Measured fruit osmotic pressure of pear fruits during the season. Error bars indicate standard deviations (n = 5).

late stress). Thus, lower fruit water and dry mass were observed compared to the standard conditions upon simulated phloem sugar stress. For the early stress simulation, water mass and dry mass were respectively 30% and 19% lower at the end of the season, while the late season stress decreased water mass and dry mass by 12% and 9% at the end of the season, respectively.

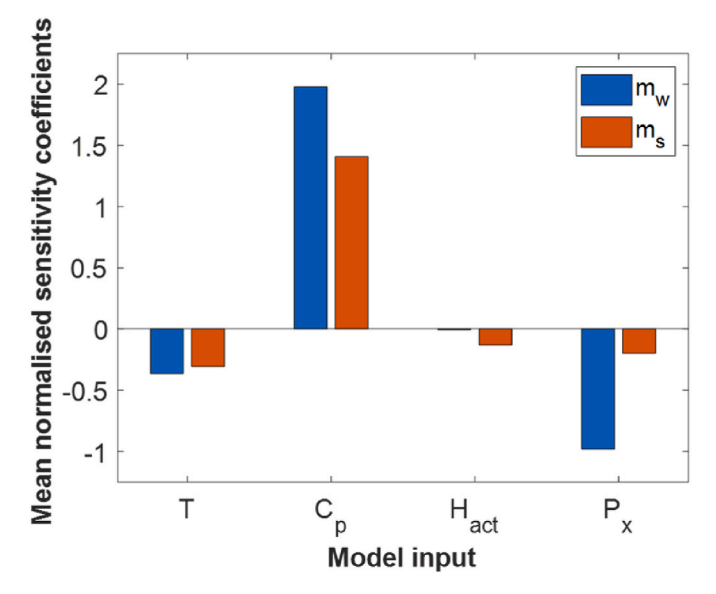


**Fig. 12.** Sensitivity analysis of the model to model inputs. Mean normalised sensitivity coefficients with respect to water mass ( $m_w$ , blue bars) and dry mass ( $m_s$ , red bars) are shown. (For interpretation of the references to colour in this figure legend, the reader is referred to the Web version of this article.)

Lower xylem water potential affected most notably fruit water mass and had limited impact on the fruit dry mass. The large decrease in fruit water (-32% during early stress and -29% during late stress) was a consequence of the decrease in the water potential gradient between xylem and phloem, and the fruit (equations (8) and (9)). Xylem flows declined by 28% during early stress and by 25% during late stress, and phloem flows similarly decreased by 25% during early stress and 18% during late stress. Respiration was only slightly lower (-3% during early stress and -1% during late stress), and transpiration as well decreased only by 8% during early stress and by 2% during late stress. Due to the lower water content and limited decrease in dry mass, fruit sugar concentration was higher than in the standard conditions, and resulted in an increase in osmotic pressure by 19% during early stress and by 4% during late stress.

# 4. Discussion

Fruit size and sugar content are important quality features that determine to a large extent their commercial value and consumer acceptance (Musacchi & Serra, 2018). The model presented in this work, based on the peach model by Fishman and Génard (1998), incorporates several adaptations to account for the specific physiology of apple and pear during growth. These modifications enabled the model to adequately simulate the seasonal patterns of apple and pear fruit growth in response to different environmental conditions during multiple seasons, as was shown in Table 1 and Fig. 1. The sensitivity analysis also showed the importance of active uptake of sugars, sugar dynamics and transport, and the water status of the branch, for the growth of apple and pear fruit. For this reason, the parameters  $L_{\rm p}$ ,  $\tau_{\rm 1}$ ,  $\tau_{\rm 2}$  and  $k_{\varphi}$  were calibrated to the data.

To incorporate the role of water status of the tree on fruit growth and its dependence on environmental conditions (Fig. 4), an empirical function was introduced to couple xylem water potential of the stem at noon with the vapour pressure deficit (equation (36)). This approach to estimate stem water potential in the 'average' branch is in line with other works, in which water potential was modeled with several different methods of varying complexity. The earliest methods (Fishman & Génard, 1998) approximated branch xylem water potential diurnal variations as sinusoidal curves during the day with a constant value for the night, and this approach has been used until today (Chen et al., 2021;

Constantinescu, Vercambre, & Génard, 2020). Other authors have presented methods based on empirical equations as function of environmental conditions such as vapour pressure deficit (Liu et al., 2007) or transpiration (Hall et al., 2013), or as function of developmental age (Jorquera-Fontena et al., 2017). Furthermore, hydraulic resistance models analogous to electric networks (Constantinescu et al., 2020; Coussement et al., 2020; Hall et al., 2013, 2017) have been developed to model water transport in response to transpiration water loss. More recently, functional-structural plant models (FSPMs) have gained attention, as they integrate 3D plant structure with plant ecophysiology to more accurately calculate local water transport (Coussement et al., 2020; Zhu et al., 2019), but are limited in simulation capabilities due to their high computational complexity. The method used in this study balances incorporating plant water status and modeling complexity, albeit without taking into account water availability.

The model was used to explore the evolution of the water (Fig. 9) and dry mass fluxes (Fig. 10), and the important fruit water status parameters during the day and over the course of the season (Fig. 11). The analysis of these variables showed that the model could produce the diurnally varying growth patterns. This result is consistent with reports for apple (Jones & Higgs, 1985; Morandi et al., 2011) and for pear (Morandi et al., 2014; Yamamoto, 1983). However, the osmotic pressure and turgor pressure inside the fruit were found to deviate from measurements (Fig. 11) and those reported in literature (Berüter, 1990; Iwanami, Moriya, & Abe, 2009). It should be noted that the aforementioned measurements of fruit turgor (except by Berüter (1990)) were performed on isolated tissue slices without the mechanical constraints of the fruit skin and might, therefore, underestimate the actual pressure. Also, (Berüter, 1990) found that apple fruit turgor remains practically constant during development. The increase in turgor pressure during growth from the simulations might be caused by the decline of cell wall extensibility, as incorporated via equation (35). Further work should aim to explore further the role of elastic deformation during growth, as the simulated water balances were sensitive to elasticity. In this context, water balance and xylem and phloem transport measurements during the day during the course of the season, similar to the methods used by Morandi et al. (2014), and measurements of the elastoplastic deformation of the fruit would be useful to quantify the fluxes relevant for water transport, and hence aid in further model development (Lechaudel et al., 2007). Fruit growth was also sensitive to cell wall extensibility. The ability of the cell wall to grow combines mechanical properties and wall-loosening processes, which are controlled hormone-regulated actions of cell wall polymer modifying enzymes (Cosgrove, 2016, 2018). The model might be improved by considering the representation of hormonal and enzymatic control of cell wall extensibility during the season (Dheilly et al., 2016; Yang et al., 2018).

The analysis of fruit growth during virtual water and carbon stress limitations illustrated the ability of the model to study complex responses to environmental and plant factors, although further experimental effort is needed to validate the stress condition simulations and potential physiological adaptations to the stresses. For instance, interventions such as covering with shading nets and under photovoltaic panels or leaf thinning have been shown to affect carbon assimilation and consequently fruit size and quality during apple fruit growth. Under such conditions, carbon supply is often limited through reduced photosynthesis, resulting in lower phloem transport, which may limit fruit size and sugar content (Juillion et al., 2022, 2023; Morandi et al., 2011). In addition, the model may also be applied to identify the impact of variations in environmental factors, such as drought stress or, which impacts plant water potential and stem flows. In turn, water stress results in smaller fruits with higher dry mass proportion (Bhusal et al., 2019; Naor et al., 1995). Similar responses and evolutions in the main components of fruit growth were obtained in the virtual stress simulations as presented in section 3.6, and hence, the model may prove to be useful to quantify and optimise the effects of such growing conditions.

Most of the adaptations for the model parameters incorporate fruit

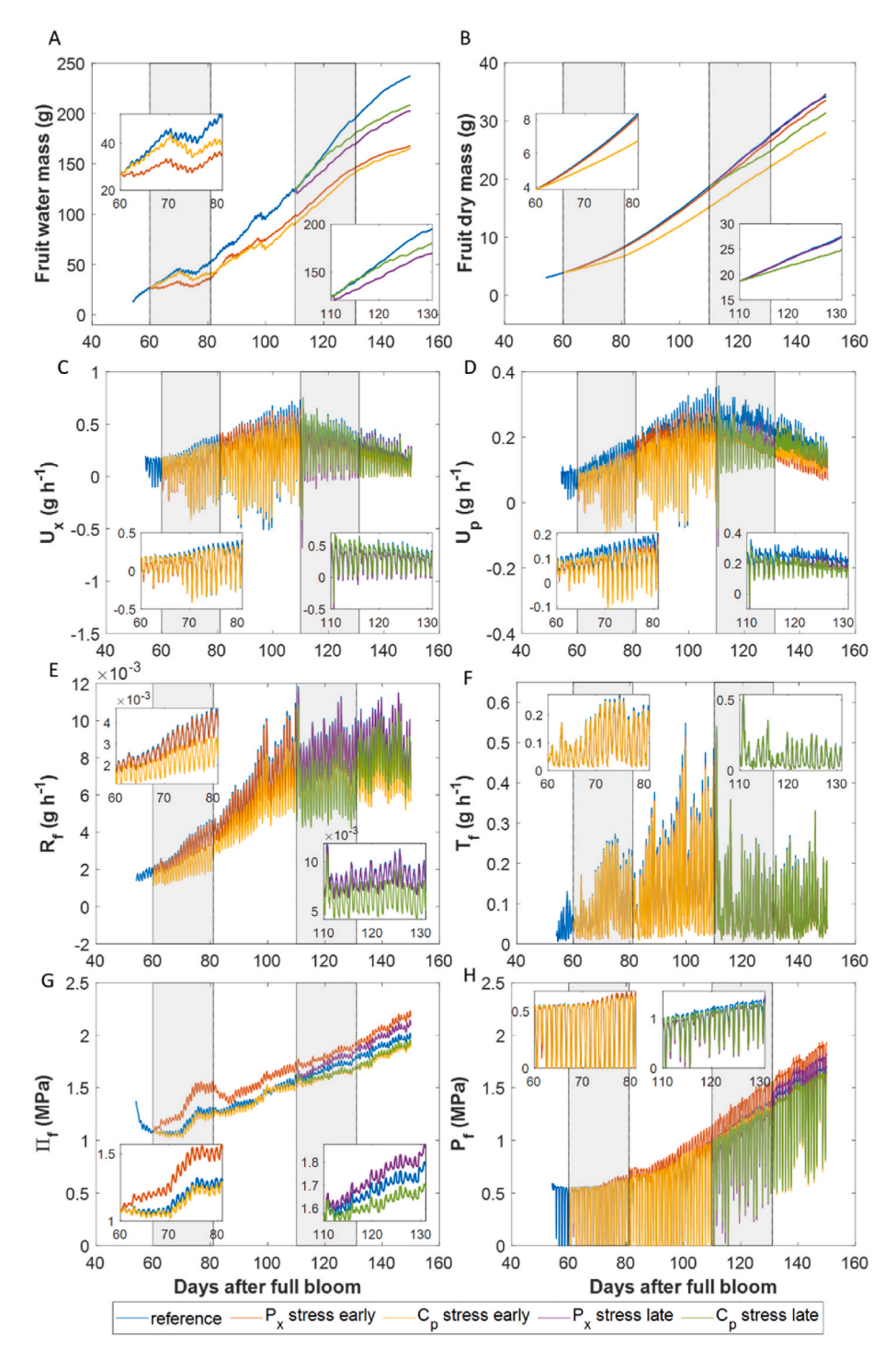


**Fig. 13.** Fruit growth dynamics simulated under reference conditions (blue line), early xylem water potential stress (red line), early phloem sugar stress (yellow line), late xylem water potential stress (purple line), and late phloem sugar stress (green line). The grey shaded areas indicate the stress periods. The inset graphs show the simulations during the stress period. A: fruit water mass (g); B: fruit dry mass (g); C: Xylem water flow (g  $h^{-1}$ ); D: phloem water flow (g  $h^{-1}$ ); E: transpiration (g  $h^{-1}$ ); G: fruit osmotic pressure (MPa); H: fruit turgor pressure (MPa). (For interpretation of the references to colour in this figure legend, the reader is referred to the Web version of this article.)

physiological processes during growth through empirical functions. These functions introduced time dependencies of these parameters, either explicitly (for example for  $L_x$  (equation (17)) and  $\varphi$  (equation (35)) or implicitly through fruit mass, as for example for Z (equation (16)) or h (equations (20) and (21)). Although the model could adequately reproduce the fruit growth patterns and was validated for an additional season, the current implementation of these parameters limits the predictive potential of the model and its interpretability. Further

research should aim to describe the processes and their parameters through additional balance equations or differential equations.

The simplified approach to model sugar dynamics yielded satisfactory results for simulations of soluble solids in apple, except late in the season. While satisfactory for pear, a decrease in osmotic pressure early in the season was found in the simulations, however. Significant differences between model predictions and measurements of osmotic pressure were found for apple as well. The underestimations were

attributed to the current implementation of sugar partitioning through  $C_{\rm f}$ , which is a function of Z. The weak linear trend observed in Z was found as the cause of the late-season differences: the model implementation of Z as constant does not account for the increase in soluble solids with respect to the total solid content late in the season. In fact, the soluble solids mass increased at the end the season due to the breakdown of starch to sugars. These trends have been observed in apple (Cakpo et al., 2020; Jing & Malladi, 2020; Li et al., 2018) and pear fruit (Oikawa et al., 2015). The fruit osmotic pressure was found to be sensitive to variations in Z, as Z strongly affected water accumulation, and hence may cause the dilution of sugars (equation (15)) and the decrease in osmotic pressure in the fruit (Figs. S3-S6). A modest improvement to fruit osmotic pressure was achieved with the implementation of Z as linear (Fig. S7); however, differences between simulation and measurement were still highest early in the season. More detailed descriptions of the fruit sugar dynamics during development, such as the models proposed by Cakpo et al. (2020) and Hall et al. (2013), may provide better representation of sugar accumulation and partitioning, and may consequently improve simulations of osmotic pressure. Simulated fruit sugar concentrations would enable better calculation of fruit osmotic pressure (equation (13)) and direct calculation of fruit soluble solids without Z.

The model presented here accounted for changes in temperature and relative humidity. Solar irradiation was found to differ considerably between different seasons (Table 1). As solar irradiation affects carbon allocation to the fruit and in turn fruit growth and quality (Corelli-Grappadelli & Lakso, 2004; Kviklys et al., 2022), further research should aim to integrate carbon supply from solar irradiation such as the models by Pallas et al. (2016) and Reyes et al. (2020) with the growth model presented here. Better representation of the effect of light perception in the canopy and carbon allocation on fruit quality and growth, could guide orchard management practices, for example fruit growth under shading nets or photovoltaic panels, and after thinning.

# 5. Conclusions

In this work, a fruit growth model for apple and pear was presented, that can simulate the accumulation of fresh mass, dry mass, and soluble solids during development for different seasons. Model modifications taking into account the particular physiology of growing apple and pear fruit were introduced. The model was shown to be highly sensitive to parameters involved in active transport, the plant water potential, dry mass transport and cell wall extensibility. Virtual water and phloem sugar stress simulations showed the response in fruit growth dynamics. Further steps include the refinement and validation of specific submodels related to cell wall changes and sugar conversion, and further investigation of the contributions of different processes during growth and in response to changing environmental factors. In the future, the model might aid in identifying and predicting optimal fruit growing management strategies.

# **Author contributions**

BD: Conceptualisation, Methodology, Investigation, Formal analysis, Writing.

JS: Investigation, Methodology, Writing – review & editing.

MR: Investigation, Methodology, Writing – review & editing.

PV: Supervision, Conceptualisation, Data curation, Writing – review & editing.

BN: Project administration, Conceptualisation, Resources, Writing  ${\mbox{-}}$  review & editing.

# Declaration of competing interest

The authors declare that they have no known competing financial interests or personal relationships that could have appeared to influence the work reported in this paper.

# Acknowledgments

BD is a PhD student funded by Research Foundation Flanders – FWO Vlaanderen (FR scholarship no. 1189422N). JS is a PhD student funded by Research Foundation Flanders – FWO Vlaanderen (SB scholarship no. 1SE1921N). This research was supported by Flanders Innovation and Entrepreneurship (VLAIO project 2015.08.95).

The help of Hans Van Cauteren and Leroi Pols during experimental data collection is gratefully acknowledged. The authors are grateful for the help of Jef Vercammen of pcfruit in enabling access to the experimental sites and plant material.

### Appendix A. Supplementary data

Supplementary data to this article can be found online at https://doi.org/10.1016/j.biosystemseng.2024.02.003.

#### References

- Berüter, J. (1990). Carbohydrate partitioning and changes in water relations of growing apple fruit. *Journal of Plant Physiology*, *135*(5), 583–587. https://doi.org/10.1016/S0176-1617(11)80640-1
- Berüter, J., Feusi, M. E. S., & Ruedi, P. (1997). Sorbitol and sucrose partitioning in the growing apple fruit. *Journal of Plant Physiology*, 151(3), 269–276. https://doi.org/ 10.1016/S0176-1617(97)80252-0
- Bhusal, N., Su Gon, H., & Yoon, T. M. (2019). Impact of drought stress on photosynthetic response, leaf water potential, and stem sap flow in two cultivars of bi-leader apple trees (Malus × Domestica Borkh.). Scientia Horticulturae, 246(July 2018), 535–543. https://doi.org/10.1016/j.scienta.2018.11.021
- Buck, A. L. (1981). New equations for computing vapor pressure and enhancement factor. *Journal of Applied Meteorology and Climatology*, 20(12), 1527–1532. https://doi.org/10.1175/1520-0450(1981)020<1527:NEFCVP>2.0.CO:2
- Bussières, P. (1994). Water import rate in tomato fruit: A resistance model. Annals of Botany, 73, 75–82.
- Cakpo, C. B., Vercambre, G., Baldazzi, V., Roch, L., Dai, Z., Valsesia, P., ... Génard, M. (2020). Model-assisted comparison of sugar accumulation patterns in ten fleshy fruits highlights differences between herbaceous and woody species. *Annals of Botany*, 126(3), 455–470. https://doi.org/10.1093/aob/mcaa082
- Chen, J., Beauvoit, B., Génard, M., Colombié, S., Moing, A., Vercambre, G., ... Dai, Z. (2021). Modelling predicts tomatoes can Be bigger and sweeter if biophysical factors and transmembrane transports are fine-tuned during fruit development. New Phytologist, 230(4), 1489–1502. https://doi.org/10.1111/nph.17260
- Christodoulou, M. D., & Culham, A. (2021). When do apples stop growing, and why does it matter? PLoS One, 16(6 June), 1–10. https://doi.org/10.1371/journal. pone.0252288
- Constantinescu, D. (2020). Analysis and improvement of a process-based model of fruit growth and composition to explore genetic variability of fruit growth mechanisms: Design ideotypes and analyze the effects of water transfers and solutes concentrations on fruit growth. PhD thesis, Université d'Avignon, Avignon, France.
- Constantinescu, D., Vercambre, G., & Génard, M. (2020). Model-assisted analysis of the peach pedicel-fruit system suggests regulation of sugar uptake and a water-saving strategy. *Journal of Experimental Botany*, 71(12), 3463–3474. https://doi.org/ 10.1093/jxb/eraa103
- Corelli-Grappadelli, L., & Lakso, A. N. (2004). Fruit development in deciduous tree crops as affected by physiological factors and environmental conditions. *Acta Horticulturae*, 636, 425–441. https://doi.org/10.17660/ActaHortic.2004.636.52
- Cosgrove, D. J. (1993). Wall extensibility: Its nature, measurement and relationship to plant cell growth. *New Phytologist*, 124, 1–23.
- Cosgrove, D. J. (2016). Plant cell wall extensibility: Connecting plant cell growth with cell wall structure, mechanics, and the action of wall-modifying enzymes. *Journal of Experimental Botany*, 67(2), 463–476. https://doi.org/10.1093/jxb/erv511
- Cosgrove, D. J. (2018). Diffuse growth of plant cell walls. Plant Physiology, 176(1), 16–27. https://doi.org/10.1104/pp.17.01541
- Coussement, J. R., De Swaef, T., Lootens, P., & Steppe, K. (2020). Turgor-driven plant growth applied in a soybean functional-structural plant model. *Annals of Botany, 126* (4), 729–744. https://doi.org/10.1093/aob/mcaa076
- De Swaef, T., Steppe, K., & Lemeur, R. (2009). Determining reference values for stem water potential and maximum daily trunk shrinkage in young apple trees based on plant responses to water deficit. Agricultural Water Management, 96(4), 541–550. https://doi.org/10.1016/j.agwat.2008.09.013
- Dheilly, E., Le Gall, S., Charlotte Guillou, M., Renou, J. P., Bonnin, E., Orsel, M., & Lahaye, M. (2016). Cell wall dynamics during apple development and storage involves hemicellulose modifications and related expressed genes. *BMC Plant Biology*, 16(201). https://doi.org/10.1186/s12870-016-0887-0
- Dražeta, L., Lang, A., Hall, A. J., Volz, R. K., & Jameson, P. E. (2004). Causes and effects of changes in xylem functionality in apple fruit. *Annals of Botany*, 93(3), 375–382. https://doi.org/10.1093/aob/mch040

- Fishman, S., & Génard, M. (1998). A biophysical model of fruit growth: Simulation of seasonal and diurnal dynamics of mass. Plant, Cell and Environment, 21, 739–752.
- Génard, M., Bertin, N., Borel, C., Bussières, P., Gautier, H., Habib, R., Léchaudel, M., Lecomte, A., Lescourret, F., Lobit, P., & Quilot, B. (2007). Towards a virtual fruit focusing on quality: Modelling features and potential uses. *Journal of Experimental Botany*, 58(5), 917–928. https://doi.org/10.1093/jxb/erl287
- Génard, M., Lescourret, F., Gomez, L., & Habib, R. (2003). Changes in fruit sugar concentrations in response to assimilate supply, metabolism and dilution: A modeling approach applied to peach fruit (*Prunus persica*). Tree Physiology, 23, 373–385.
- Hall, A. J., Minchin, P. E. H., Gould, N., & Clearwater, M. J. (2017). A biophysical model of fruit development with distinct apoplasmic and symplasmic pathways. *Acta Horticulturae*, 1160(2013), 367–374. https://doi.org/10.17660/ ActaHortic.2017.1160.53
- Hall, A., Peter, M., Clearwater, M., & Génard, M. (2013). A biophysical model of kiwifruit (Actinidia deliciosa) berry development. Journal of Experimental Botany, 64(18), 5473–5483. https://doi.org/10.1093/ixb/ert317
- Hall, A. J., Richardson, A. C., & Snelgar, W. P. (2006). Modelling fruit development in 'hayward' kiwifruit. Acta Horticulturae, 707(1997), 41–47. https://doi.org/ 10.17660/ActaHortic.2006.707.4
- Hertog, M. L. A. T. M., Verlinden, B. E., Lammertyn, J., & Nicolaï, B. M. (2007). OptiPa, an essential primer to develop models in the postharvest area. *Computers and Electronics in Agriculture*, 57(1), 99–106. https://doi.org/10.1016/j.compag.2007.02.001
- Iwanami, H., Moriya, S., & Abe, K. (2009). Relationships between sap flow, hydraulic conductivity, and the anatomical characteristics of stems and roots in apple rootstocks of different vigour. The Journal of Horticultural Science and Biotechnology, 84(6), 632–638. https://doi.org/10.1080/14620316.2009.11512578
- Iwanami, H., Moriya, S., Kotoda, N., & Abe, K. (2008). Turgor closely relates to postharvest fruit softening and can be a useful index to select a parent for producing cultivars with good storage potential in apple. *HortScience*, 43(5), 1377–1381. https://doi.org/10.21273/hortsci.43.5.1377
- Janssen, B. J., Kate Thodey, Schaffer, R. J., Alba, R., Balakrishnan, L., Bishop, R., Bowen, J. H., Crowhurst, R. N., Gleave, A. P., Ledger, S., Steve McArtney, Pichler, F. B., Snowden, K. C., & Ward, S. (2008). Global gene expression analysis of apple fruit development from the floral bud to ripe fruit. BMC Plant Biology, 8, 1–29. https://doi.org/10.1186/1471-2229-8-16
- Jing, S., & Malladi, A. (2020). Higher growth of the apple (Malus × Domestica Borkh.) Fruit cortex is supported by resource intensive metabolism during early development. *BMC Plant Biology*, 20(1), 1–19. https://doi.org/10.1186/s12870-020-2280-2
- Jones, H. G., & Higgs, K. H. (1982). Surface conductance and water balance of developing apple (*Malus pumila mill.*) fruits. *Journal of Experimental Botany*, 33(1), 67–77. https://doi.org/10.1093/jxb/33.1.67
- Jones, H. G., & Higgs, K. H. (1985). Water movement into and out of apple fruits. Acta Horticulturae, 171, 353–359.
- Jorquera-Fontena, E., Génard, M., & Franck, N. (2017). Analysis of blueberry (vaccinium corymbosum l.) fruit water dynamics during growth using an ecophysiological model. *The Journal of Horticultural Science and Biotechnology*, 92(6), 646–659. https://doi.org/10.1080/14620316.2017.1304810
- Juillion, P., Lopez, G., Fumey, D., Génard, M., & Vercambre, G. (2023). Analysis and modelling of tree shading impacts on apple fruit quality: Case study with an agrivoltaic system. Acta Horticulturae, 1366, 187–194. https://doi.org/10.17660/ ActaHortic.2023.1366.21
- Juillion, P., Lopez, G., Fumey, D., Vincent, L., Génard, M., & Vercambre, G. (2022). Shading apple trees with an agrivoltaic system: Impact on water relations, leaf morphophysiological characteristics and yield determinants. *Scientia Horticulturae*, 306(July). https://doi.org/10.1016/j.scienta.2022.111434
- Knipfer, T., & Fricke, W. (2010). Root pressure and a solute reflection coefficient close to unity exclude a purely apoplastic pathway of radial water transport in barley (Hordeum vulgare). New Phytologist, 187(1), 159–170. https://doi.org/10.1111/ i.1469-8137.2010.03240.x
- Kviklys, D., Jonas, V., Liaudanskas, M., Janulis, V., Laužikė, K., Samuolienė, G., Uselis, N., & Lanauskas, J. (2022). Apple fruit growth and quality depend on the position in tree canopy. *Plants*, 11(2). https://doi.org/10.3390/plants11020196
- Lakso, A. N., Grappadelli, L. C., Barnard, J., & Goffinet, M. C. (1995). An expolinear model of the growth pattern of the apple fruit. *Journal of Horticultural Science*, 70(3), 389–394. https://doi.org/10.1080/14620316.1995.11515308
- Lang, A. (1990). Xylem, phloem and transpiration flows in developing apple fruits. Journal of Experimental Botany, 41(6), 645–651. https://doi.org/10.1093/jxb/
- Léchaudel, M., Génard, M., Lescourret, F., Urban, L., & Jannoyer, M. (2005). Modeling effects of weather and source-sink relationships on mango fruit growth. *Tree Physiology*, 25(5), 583–597. https://doi.org/10.1093/treephys/25.5.583
- Lechaudel, M., Vercambre, G., Lescourret, F., Normand, F., & Génard, M. (2007). An analysis of elastic and plastic growth of mango in response to various assimilate supplies. *Tree Physiology*, 27, 219–230.
- Lescourret, F., Mimoun, M. B., & Génard, M. (1998). A simulation model of growth at the shoot-bearing fruit level i. description and parameterization for peach. *European Journal of Agronomy*, 9(2–3), 173–188. https://doi.org/10.1016/S1161-0301(98) 00035-5
- Levin, A. D. (2019). Re-evaluating pressure chamber methods of water status determination in field-grown grapevine (Vitis Spp.). Agricultural Water Management, 221, 422–429. https://doi.org/10.1016/j.agwat.2019.03.026. October 2018.

- Li, M., Li, P., Ma, F., Dandekar, A. M., & Cheng, L. (2018). Sugar metabolism and accumulation in the fruit of transgenic apple trees with decreased sorbitol synthesis. Horticulture Research, 5(1). https://doi.org/10.1038/s41438-018-0064-8
- Liu, H. F., Génard, M., Guichard, S., & Bertin, N. (2007). Model-assisted analysis of tomato fruit growth in relation to carbon and water fluxes. *Journal of Experimental Botany*, 58(13), 3567–3580. https://doi.org/10.1093/jxb/erm202
- Lockhart, J. A. (1965). An analysis of irreversible plant cell elongation. Journal of Theoretical Biology, 8(2), 264–275. https://doi.org/10.1016/0022-5193(65)90077-9
- Łysiak, G. P. (2022). Degree days as a method to estimate the optimal harvest date of 'conference' pears. Agriculture, 12(11). https://doi.org/10.3390/ agriculture12111803
- Maguire, K. M., Banks, N. H., Lang, A., & Gordon, I. L. (2000). Harvest date, cultivar, orchard, and tree effects on water vapor permeance in apples. *Journal of the American Society for Horticultural Science*, 125(1), 100–104. https://doi.org/10.21273/jashs.125.1.100
- Marcelis, L. F. M., Elings, A., De Visser, P. H. B., & Heuvelink, E. (2009). Simulating growth and development of tomato crop. Acta Horticulturae, 821, 101–110. https:// doi.org/10.17660/ActaHortic.2009.821.10
- Martins, J. M. S., Rosa, A. R., Martins, S., Fialho, D., & Abreu, J. (2008). Modelling the shape and growth of a pear. Acta Horticulturae, 800(PART 1), 331–337. https://doi. org/10.17660/actahortic.2008.800.41
- Matsoukas, I. G., Massiah, A. J., & Thomas, B.. (2013). Starch metabolism and antiflorigenic signals modulate the juvenile-to-adult phase transition in arabidopsis. Plant, Cell and Environment, 36, 1802–1811. https://doi.org/10.1111/pce.12088
- Morandi, B., Losciale, P., Manfrini, L., Zibordi, M., Anconelli, S., Galli, F., Pierpaoli, E., & Grappadelli, L. C. (2014). Increasing water stress negatively affects pear fruit growth by reducing first its xylem and then its phloem inflow. *Journal of Plant Physiology*, 171(16), 1500–1509. https://doi.org/10.1016/j.jplph.2014.07.005
- Morandi, B., Zibordi, M., Losciale, P., Manfrini, L., Bastías, R. M., & Grappadelli, L. C. (2012). Apple and peach: A different role for fruit transpiration? *Acta Horticulturae*, 932(June), 213–218. https://doi.org/10.17660/ActaHortic.2012.932.30
- Morandi, B., Zibordi, M., Losciale, P., Manfrini, L., Pierpaoli, E., & Grappadelli, L. C. (2011). Shading decreases the growth rate of young apple fruit by reducing their phloem import. Scientia Horticulturae, 127(3), 347–352. https://doi.org/10.1016/j.scienta.2010.11.002
- Musacchi, S., & Serra, S. (2018). Apple fruit quality: Overview on pre-harvest factors. Scientia Horticulturae, 234(July 2017), 409–430. https://doi.org/10.1016/j. scienta.2017.12.057
- Naor, A., Klein, I., & Doron, I. (1995). Stem water potential and apple size. *Journal of the American Society for Horticultural Science*, 120(4), 577–582. https://doi.org/ 10.21273/jashs.120.4.577
- Nemeskéri, E. (2007). Water relations of apple and influence on fruit quality (Minireview). *International Journal of Horticultural Science*, 13(3), 59–63. https://doi. org/10.31421/ijhs/13/3/747
- Nobel, P. S. (1974). In D. Kennedy, & R. B. Park (Eds.), Introduction to biophysical plant physiology. San Francisco, CA: W.H. Freeman and Company.
- Oikawa, A., Otsuka, T., Nakabayashi, R., Jikumaru, Y., Isuzugawa, K., Murayama, H., Saito, K., & Shiratake, K. (2015). Metabolic profiling of developing pear fruits reveals dynamic variation in primary and secondary metabolites, including plant hormones. PLoS One. 10(7), 1–18. https://doi.org/10.1371/j.journal.pone.0131408
- Ortega, J. K. E. (1985). Augmented growth equation for cell wall expansion. Plant Physiology, 79(1), 318–320. https://doi.org/10.1104/pp.79.1.318
- Ortega, J. K. E. (1990). Governing equations for plant cell growth. *Physiologia Plantarum*, 79(1) 116–121 https://doi.org/10.1111/j.1399-3054.1990.tb05873.x
- 79(1), 116–121. https://doi.org/10.1111/j.1399-3054.1990.tb05873.x
  Pallas, B., Da Silva, D., Valsesia, P., Yang, W., Guillaume, O., Lauri, P. E., Vercambre, G., Génard, M., & Evelyne Costes. (2016). Simulation of carbon allocation and organ growth variability in apple tree by connecting architectural and source-sink models. 
  Annals of Botany, 118(2), 317–330. https://doi.org/10.1093/aob/mcw085
- Parton, W. J., & Logan, J. A. (1981). A model for diurnal variation in soil and air temperature. Agricultural Meteorology, 23(C), 205–216. https://doi.org/10.1016/ 0002-1571(81)90105-9
- Proseus, T. E., Ortega, J. K. E., & Boyer, J. S. (1999). Separating growth from elastic deformation during cell enlargement. *Plant Physiology, 119*(February), 775–784.
- Reyes, F., Pallas, B., Pradal, C., Vaggi, F., Zanotelli, D., Tagliavini, M., Gianelle, D., & Costes, E. (2020). MuSCA: A multi-scale source-sink carbon allocation model to explore carbon allocation in plants. An application to static apple tree structures. Annals of Botany, 126(4), 571–585. https://doi.org/10.1093/aob/mcz122
- Ribeiro, T. D., Villela Savian, T., Jesus Fernandes, T., & Augusto Muniz, J. (2017). The use of the nonlinear models in the growth of pears of 'shinseiki' cultivar. *Ciência Rural*, 48(1), 1–7. https://doi.org/10.1590/0103-8478cr20161097
- Rodríguez, A., Sánchez, E., & De La Casa, A. (2011). Contributions of early season temperatures to pyrus communis 'Bartlett' fruit growth. *Acta Horticulturae*, 909, 657–664.
- Rolland, F., Baena-gonzalez, E., & Jen, S. (2006). Sugar sensing and signaling in plants: Conserved and novel mechanisms. *Annual Review of Plant Biology*, 57, 675–709. https://doi.org/10.1146/annurev.arplant.57.032905.105441
- Shackel, K. A. (2007). Water relations of woody perennial plant species. *Journal International des Sciences de la Vigne et du Vin, 41*(3), 121–129. https://doi.org/10.20870/oeno-one.2007.41.3.847
- Šircelj, H., Tausz, M., Grill, D., & Batič, F. (2005). Biochemical responses in leaves of two apple tree cultivars subjected to progressing drought. *Journal of Plant Physiology*, 162 (12), 1308–1318. https://doi.org/10.1016/j.jplph.2005.01.018
- Tijero, V., Girardi, F., & Botton, A. (2021). Fruit development and primary metabolism in apple. *Agronomy*, *11*(6), 1160. https://doi.org/10.3390/agronomy11061160
- Van de Wal, B. (2017). Measuring and modelling plant-fruit interactions and fruit quality under changing water availability in tomato and grape. Ghent University.

- Vélez-Sánchez, Enrique, J., Enrique Balaguera-López, H., & Rodríguez Hernández, P. (2022). The water status of pear (*Pyrus communis l.*) under application of regulated deficit irrigation in high tropical latitudinal conditions. *Journal of the Saudi Society of Agricultural Sciences*, 21(7), 460–468. https://doi.org/10.1016/j.jssas.2021.12.003
- Wada, H., Nakata, K., Nonami, H., Erra-Balsells, R., Tatsuki, M., Hatakeyama, Y., & Tanaka, F. (2021). Direct evidence for dynamics of cell heterogeneity in watercored apples: Turgor-associated metabolic modifications and within-fruit water potential gradient unveiled by single-cell analyses. Horticulture Research, 8(1), 1–15. https://doi.org/10.1038/s41438-021-00603-1
- Yamamoto, T. (1983). Models of water competition between fruits and leaves on spurs of 'bartlett' pear trees and its measurement by a heat-pulse method. 20, 241–250.
- Yang, H., Liu, J., Dang, M., Zhang, B., Li, H., Meng, R., Dong, Q., Yang, Y., & Zhao, Z. (2018). Analysis of β-galactosidase during fruit development and ripening in two different texture types of apple cultivars. Frontiers in Plant Science, 9(April), 1–13. https://doi.org/10.3389/fpls.2018.00539
- Zadravec, P., Veberic, R., Stampar, F., Schmitzer, V., & Eler, K. (2014). Fruit growth patterns of four apple cultivars using nonlinear growth models. *European Journal of Horticultural Science*, 79(2), 52–59.
- Zhu, J., Génard, M., Poni, S., Gambetta, G. A., Vivin, P., Vercambre, G., Michael, C., Trought, T., Ollat, N., Delrot, S., & Dai, Z. (2019). Modelling grape growth in relation to whole-plant carbon and water fluxes. *Journal of Experimental Botany*, 70(9), 2505–2521. https://doi.org/10.1093/jxb/ery367